Indian Institute of Astrophysics, Bangalore, Seminar Feb. 20, 2008

On the structure of the solar internetwork magnetic field: Numerical simulations in comparison to observations with Hinode

O. Steiner

Kiepenheuer-Institut für Sonnenphysik, Freiburg i.Br., Germany

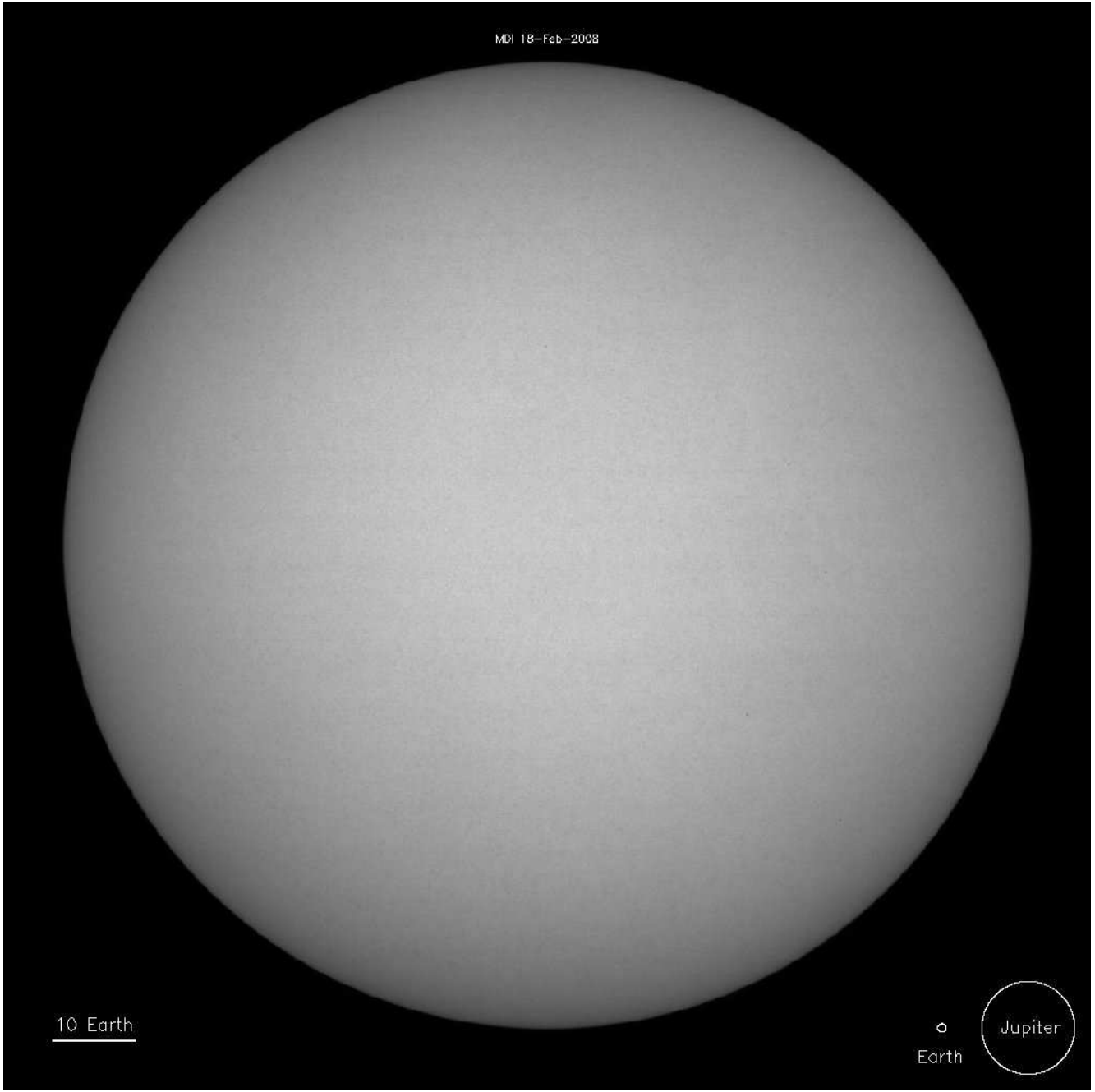
MDI 18-Feb-2008
10 Earth
Earth
Jupiter

1. Observations with Hinode

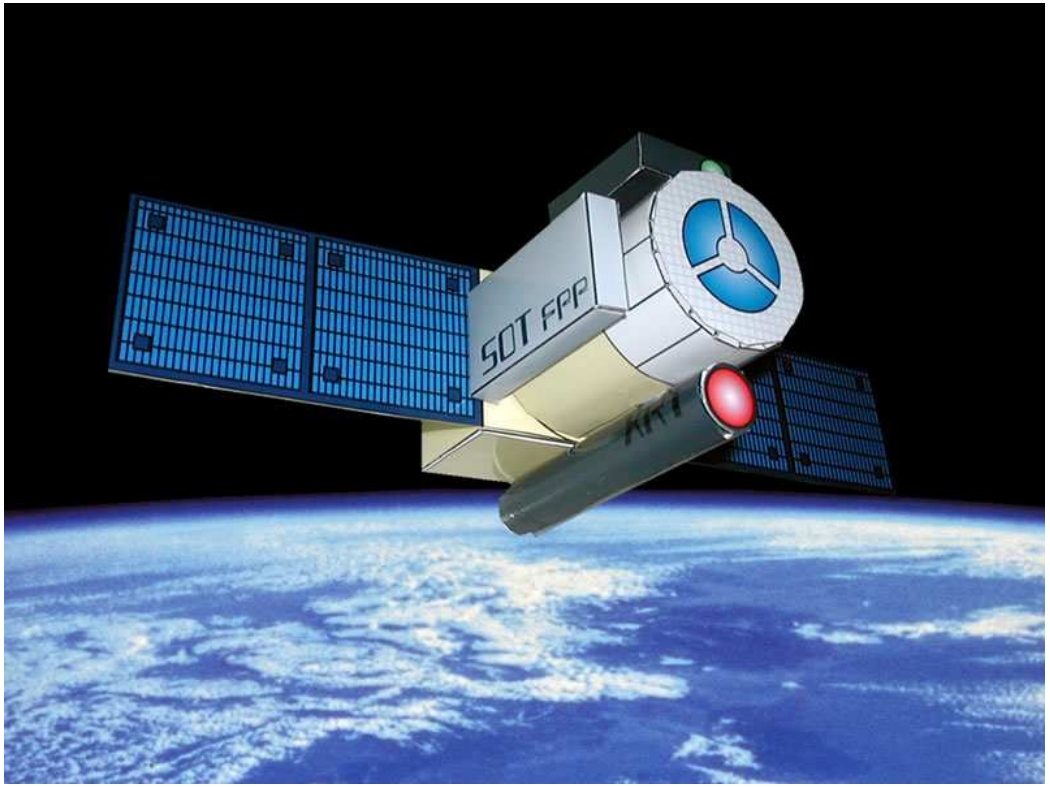

Hinode (Solar-B) launched on 22 September 2006. The Solar Optical Telescope (SOT) has an aperture of 50 cm featuring an image stabilization system consisting of a piezo-driven tip-tilt mirror. The Spectral-polarimeter (SP) generates Stokes $IQUV$ spectral images.

`http://solar-b.nao.ac.jp`

Observations with Hinode (cont.)

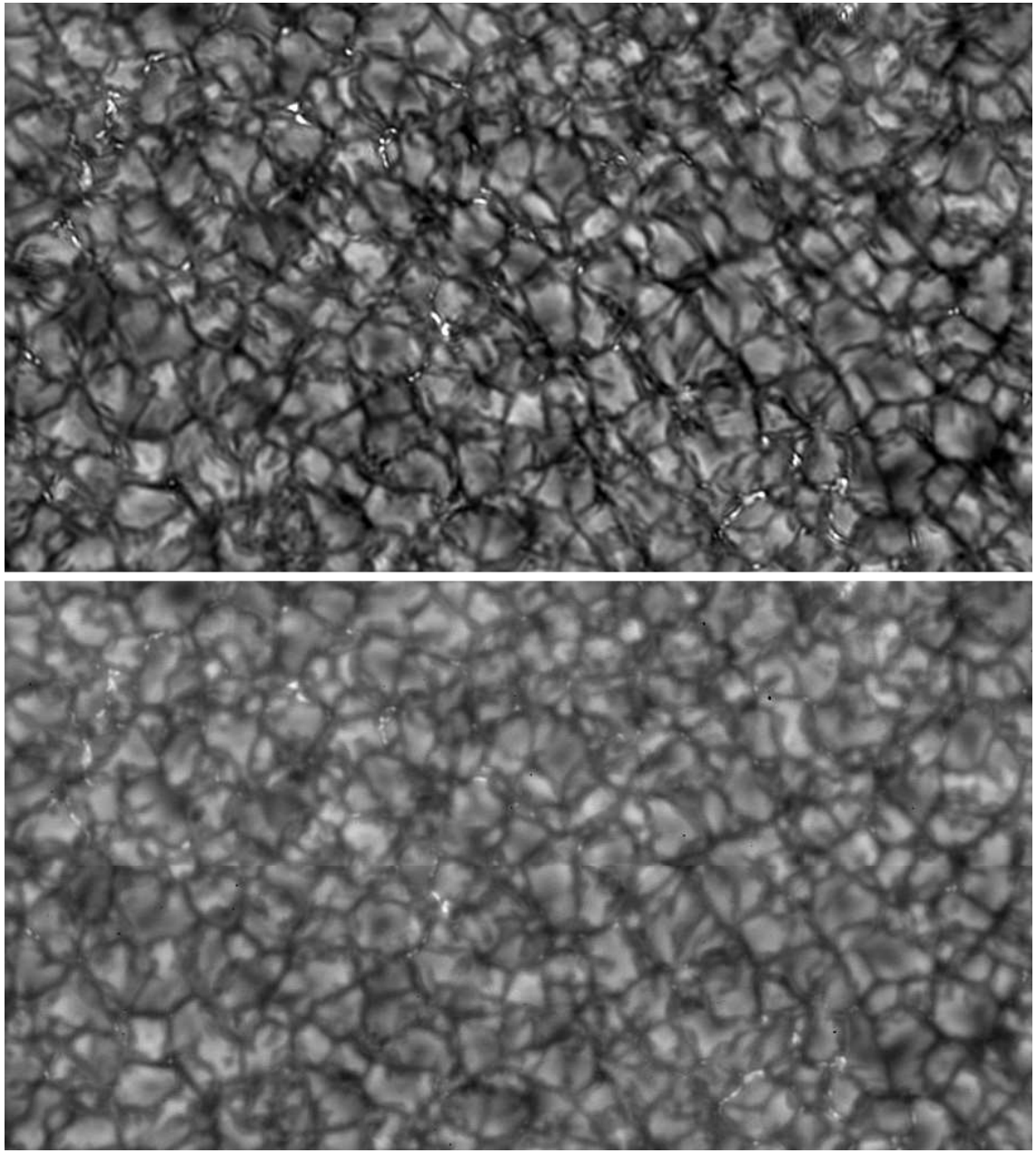

Comparison of G-band images from a ground based solar observatory (the DST) and the Hinode/SOT.

Courtesy *Friedrich Wöger and Kevin Reardon*, Sacramento Peak Observatory.

Observations with Hinode (cont.)

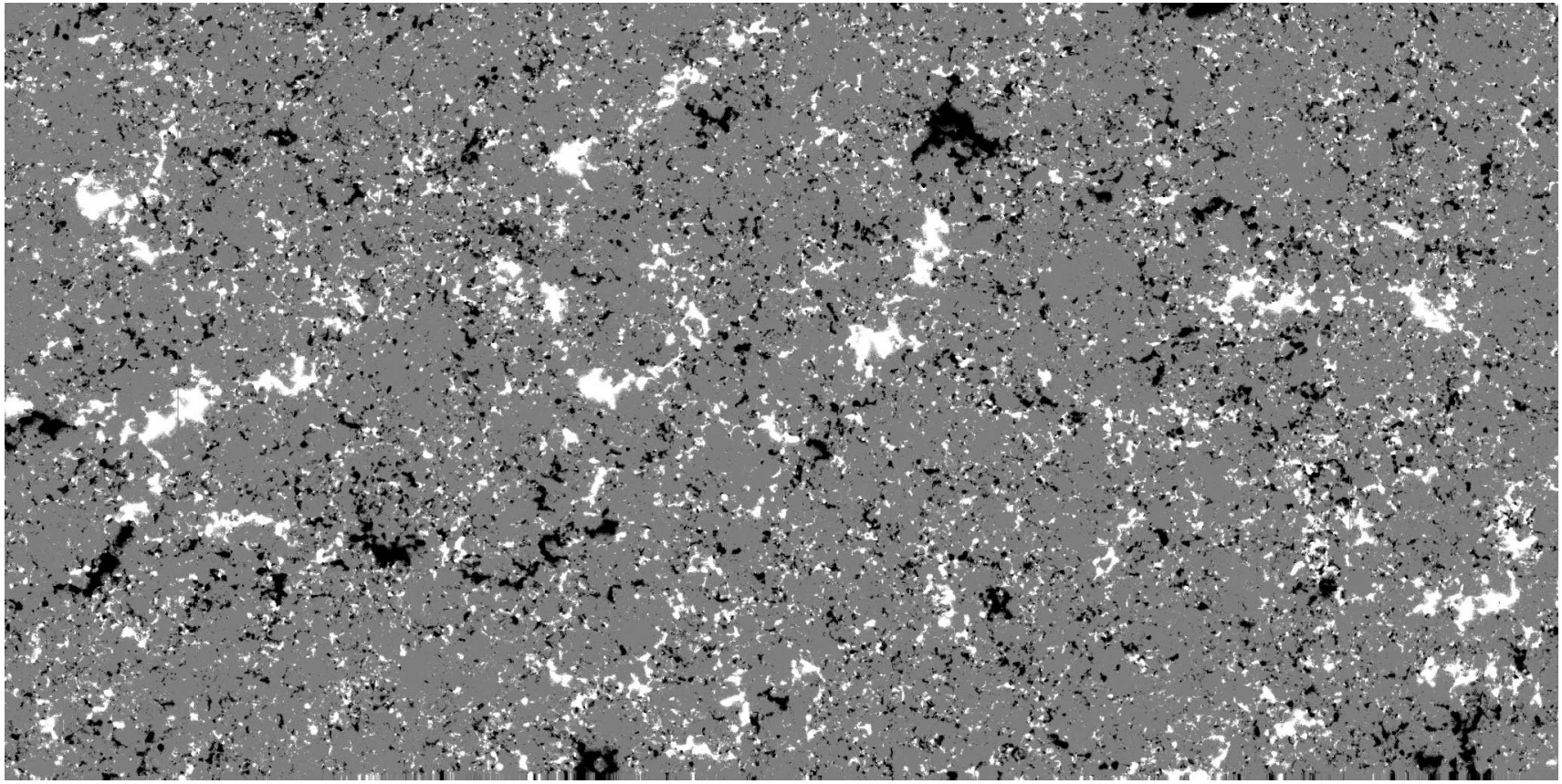

Apparent vertical magnetic flux density, $B^{\mathrm{L}}_{\mathrm{app}}$. of the quiet Sun over a field of view of $302'' \times 162''$. The grey scale saturates at ± 50 Mx cm^{-2}. 2048 steps to 5 s.

$\langle |B^{\mathrm{L}}_{\mathrm{app}}| \rangle = 11.7$ *Mx cm*$^{-2}$. From *Lites et. al. 2008, ApJ 672, 1237*

Observations with Hinode (cont.)

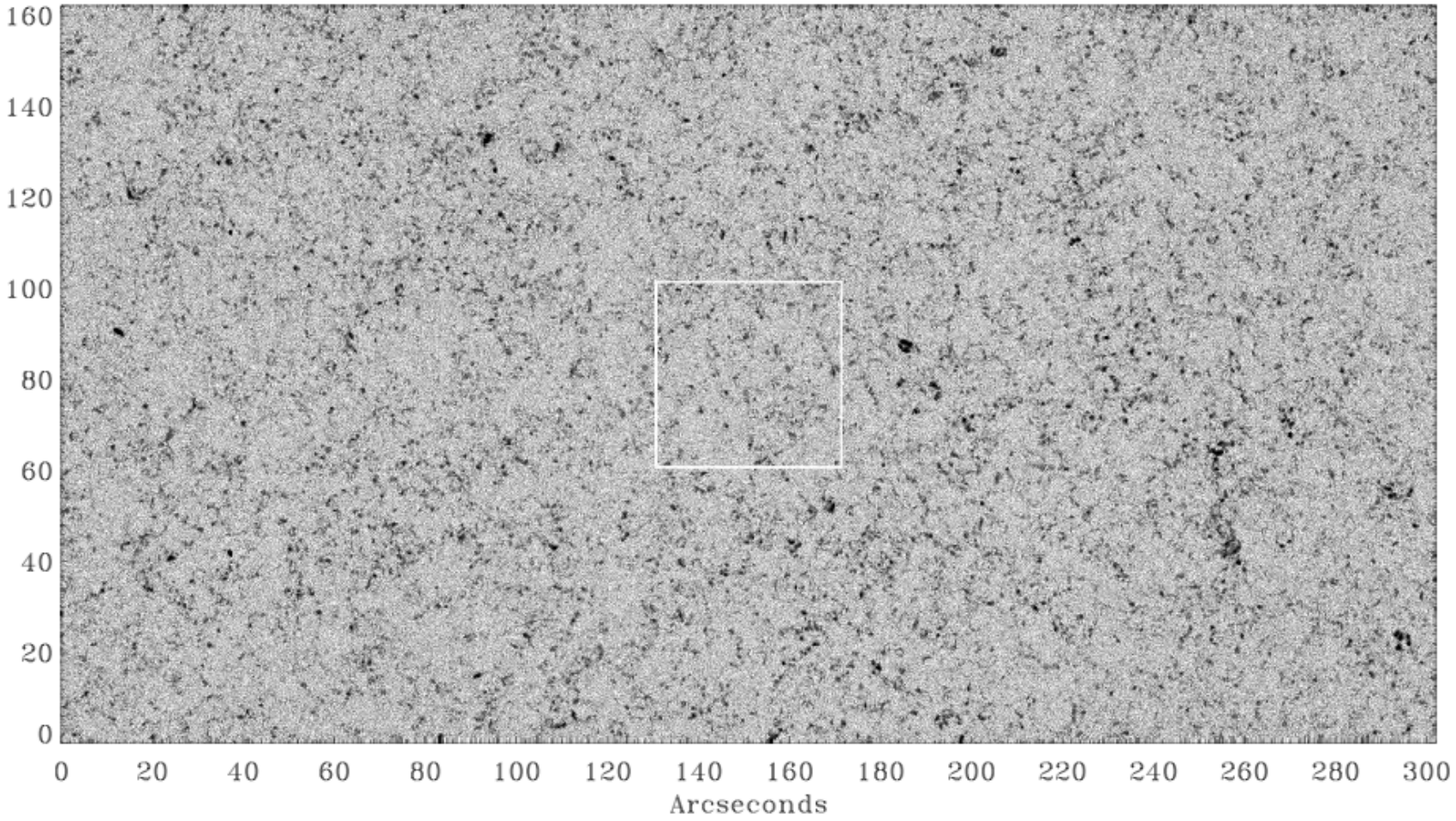

Apparent horizontal magnetic flux density, $B^{\mathrm{T}}_{\mathrm{app}}$, of the quiet Sun over a field of view of $302'' \times 162''$. The grey scale saturates at ± 200 Mx cm^{-2}. 2048 steps to 5 s.

$\langle B^{\mathrm{T}}_{\mathrm{app}} \rangle = 60.0$ *Mx cm*$^{-2}$. From *Lites et. al. 08*

Observations with Hinode (cont.)

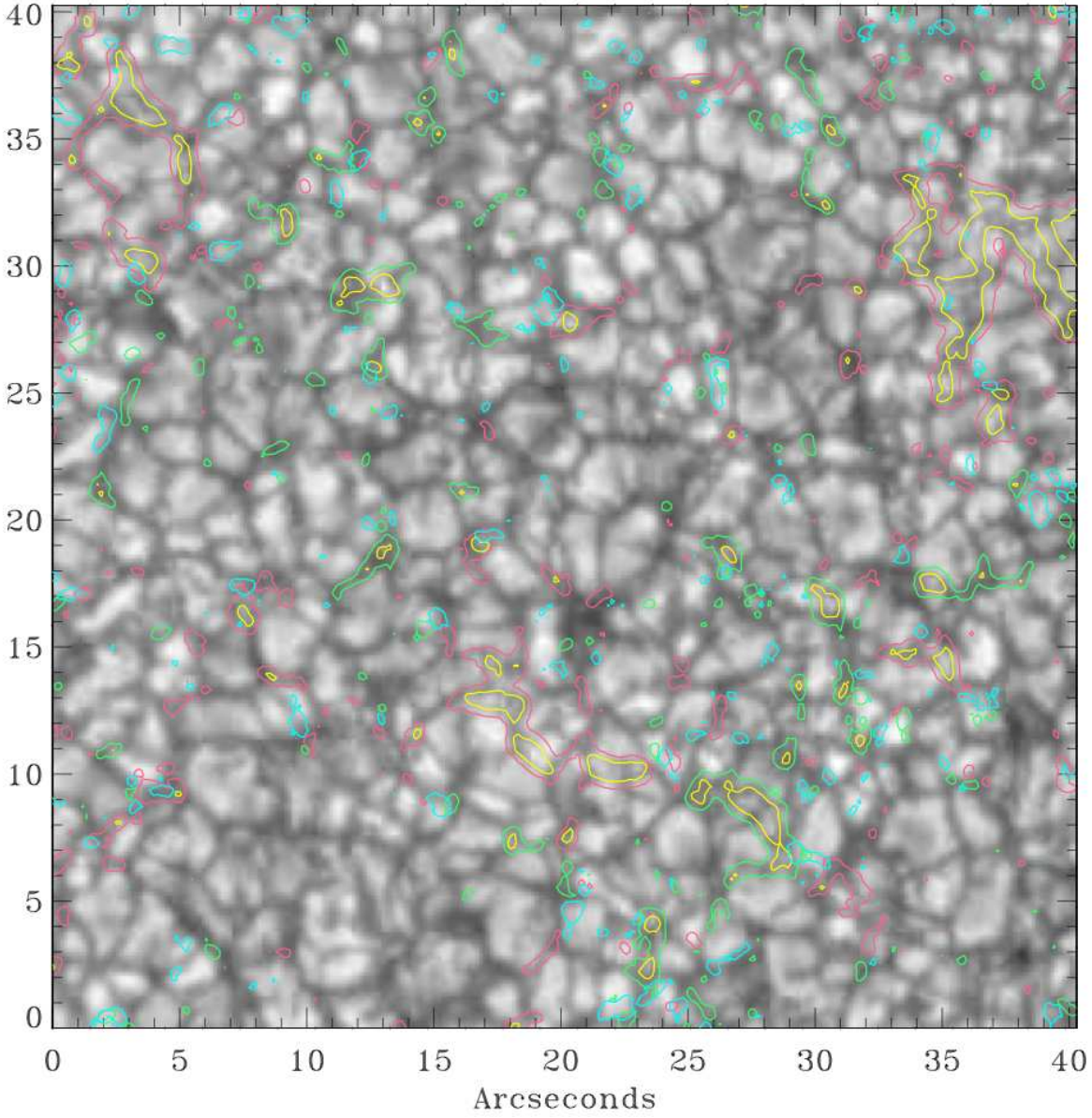

Red and *green*: contours of $B^{\mathrm{L}}_{\mathrm{app}} = 24$ Mx cm^{-2}, respectively positive and negative. *Yellow*: contours of $B^{\mathrm{L}}_{\mathrm{app}} = 100$ Mx cm^{-2}. *Blue* contours correspond to $B^{\mathrm{T}}_{\mathrm{app}} = 122$ Mx cm^{-2}. Horizontal flux preferentially occurs at locations between lanes and granule centers. From *Lites et. al. 08*

Observations with Hinode (cont.)

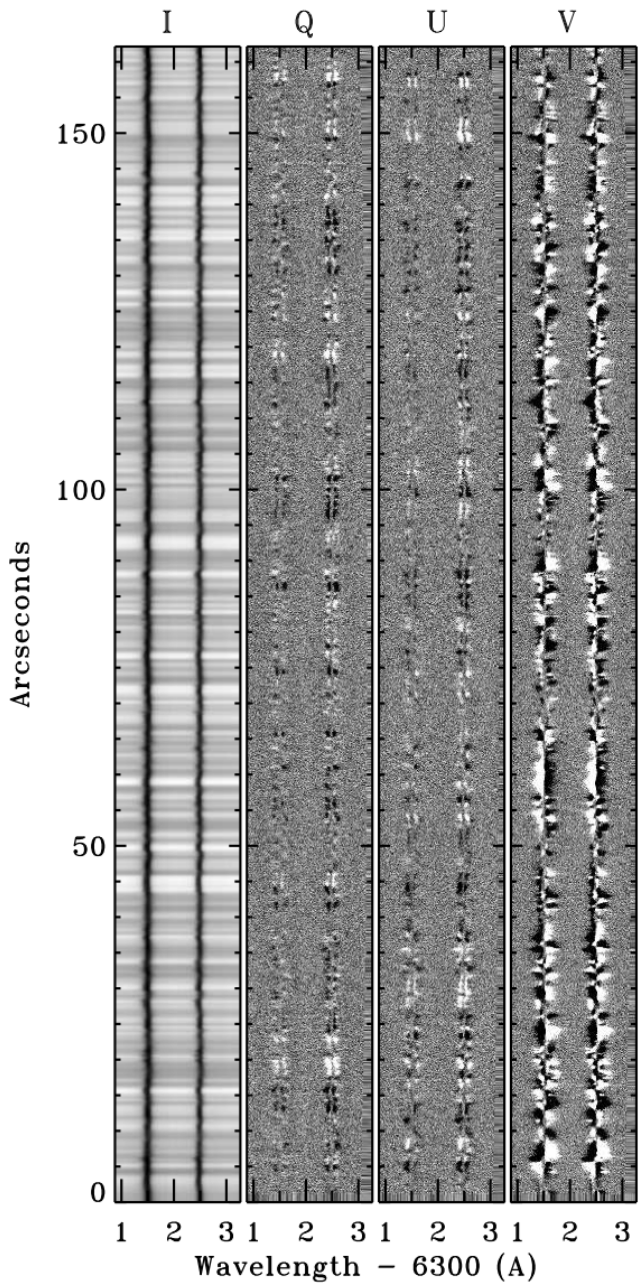

Deep mode Stokes spectra with an integration time of 67.2 s. rms polarization in the continuum of 3×10^{-4}. From a 2-hour time series Lites et al. obtain $\langle B^{\rm L}_{\rm app} \rangle = 11.0$ Mx cm^{-2}. $\langle B^{\rm T}_{\rm app} \rangle = 55.3$ Mx cm^{-2}. From *Lites et. al. 08*

2. Numerical simulation of near surface magnetoconvection

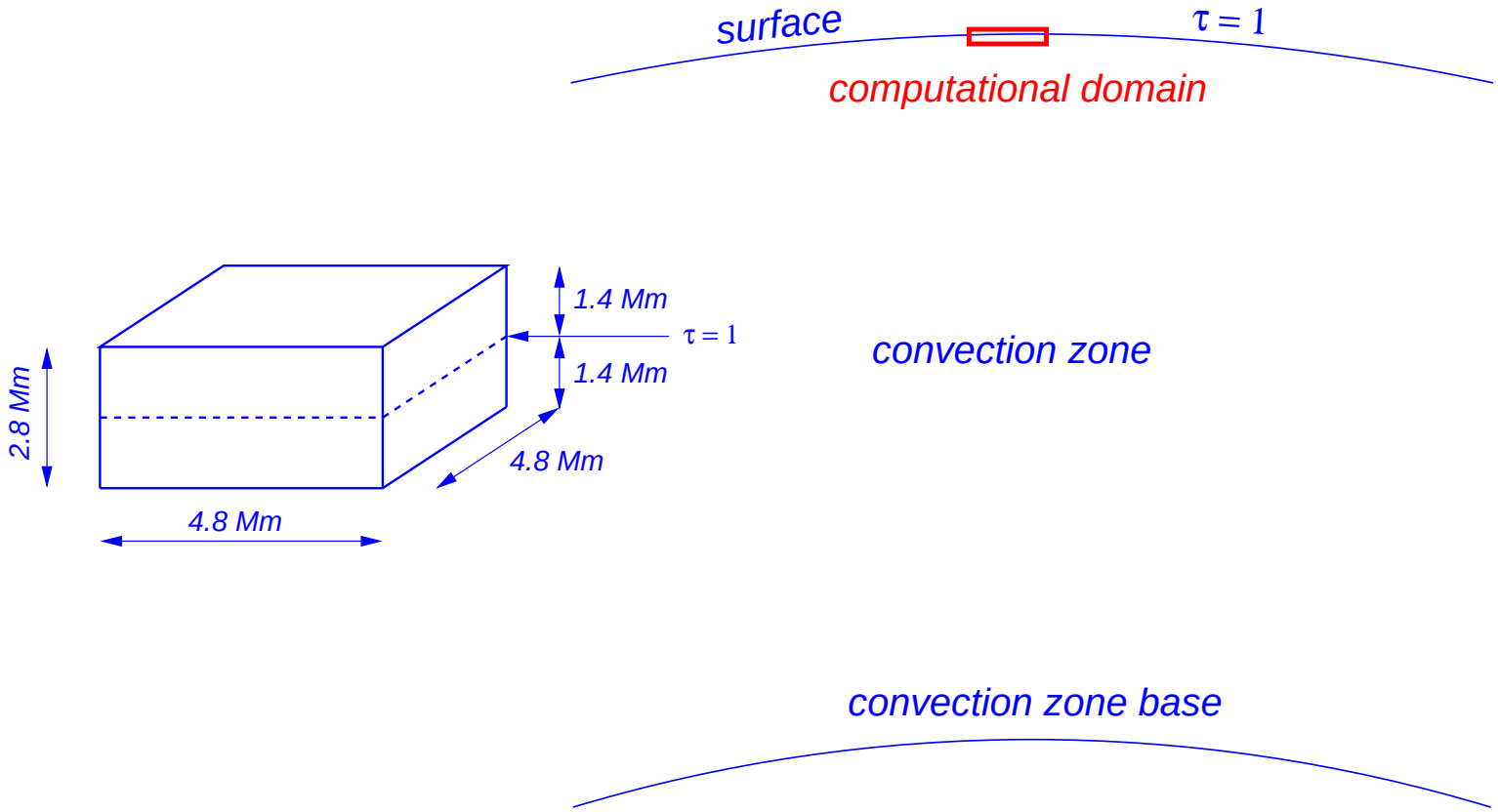

Typical size of a three-dimensional computational box (left) on scale with the convection zone boundaries (right)

Application examples of CO^{5}BOLD (Courtesy Sven Wedemeyer-Böhm)

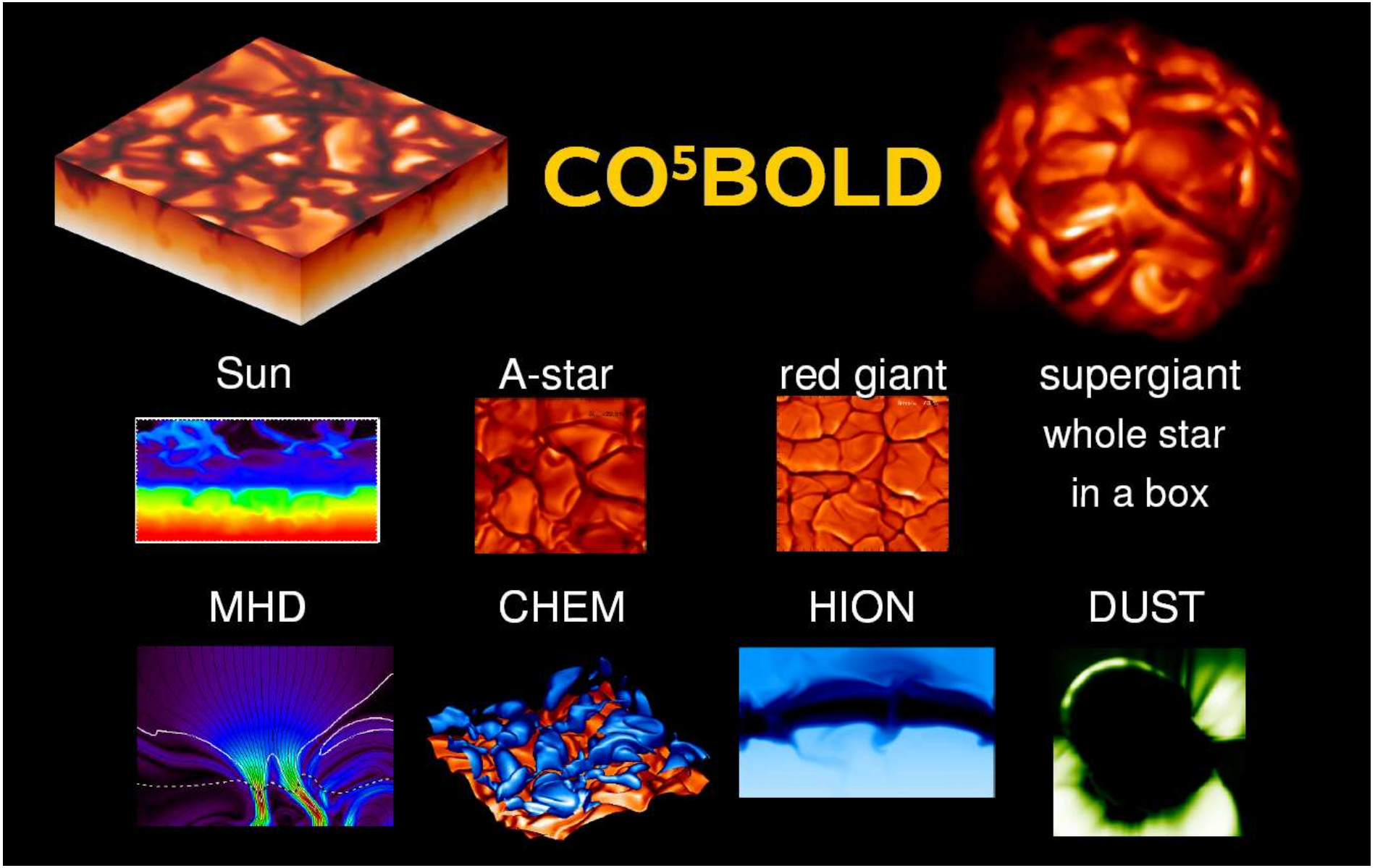

Numerical simulation of near surface magnetoconvection (cont.)

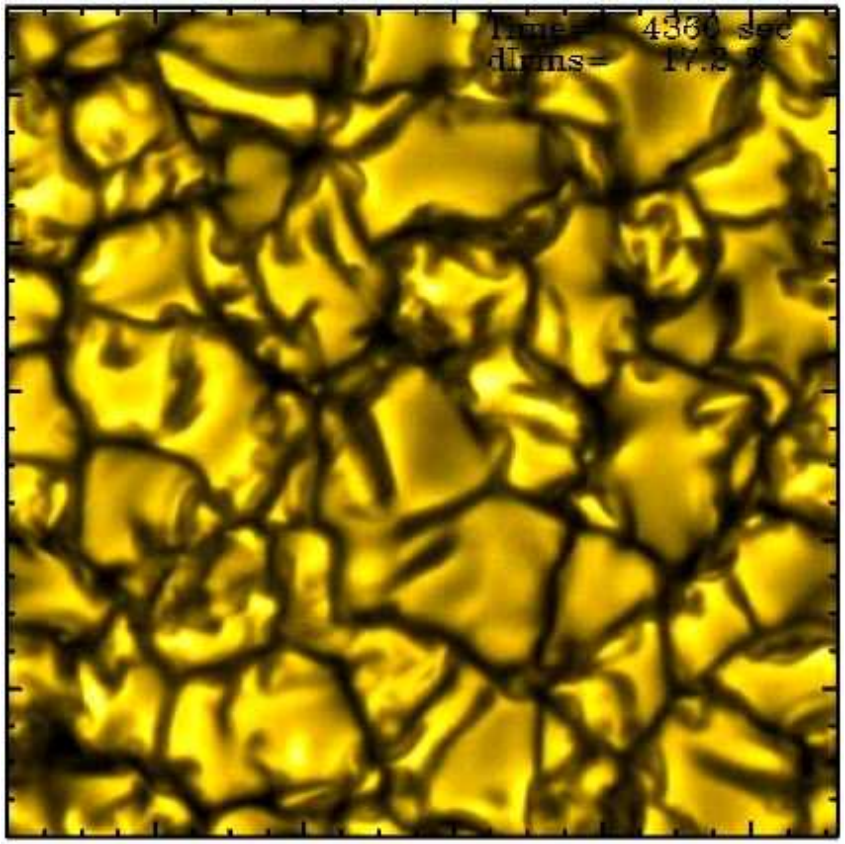

Simulation of solar granulation with CO^{5}BOLD. $400 \times 400 \times 165$ grid cells, 11.2×11.2 Mm, Mean contrast at $\lambda \approx 620$ nm is 16.65%.

Courtesy *M. Steffen, AIP*

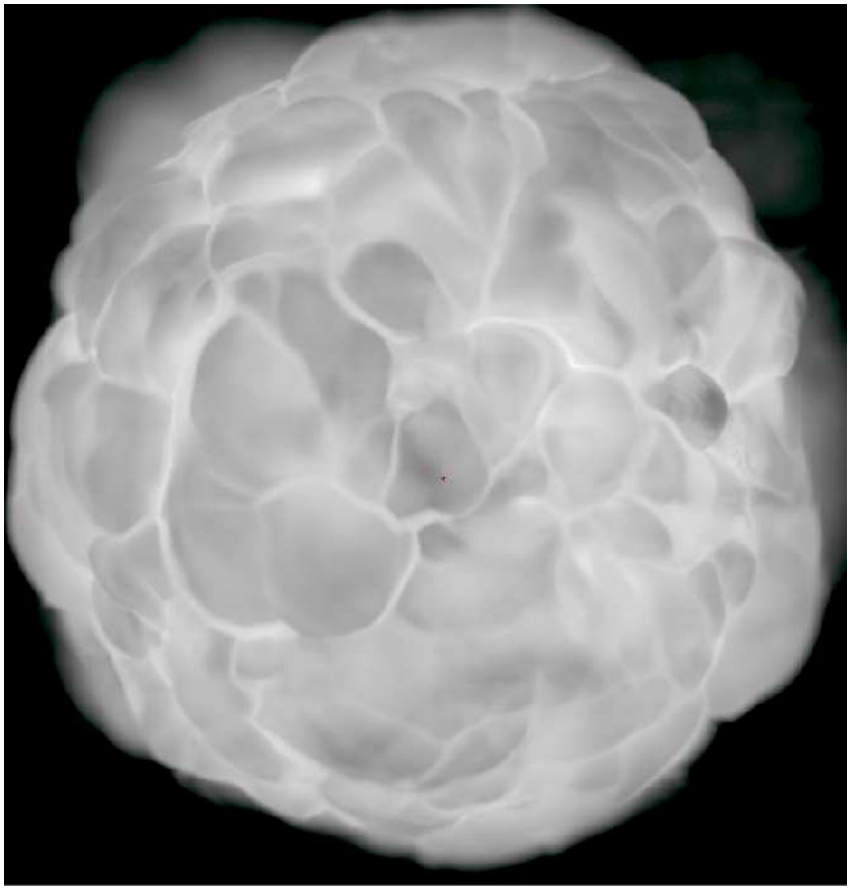

Simulation of a red supergiant with CO^{5}BOLD. 235^3 grid cells, $m_{\rm star} = 12 m_\odot$, $T_{\rm eff} = 3436$ K, $R_{\rm star} = 875 R_\odot$

Courtesy *Bernd Freytag*

Numerical simulation of near surface magnetoconvection (cont.)

Two-dimensional radiation-hydrodynamic simulation of surface convection including the chromospheric layer. The dimensions of the computational domain are: Width, 5600 km; Height above the surface of $\tau = 1$, 1700 km; Depth below this surface level: 1400 km.

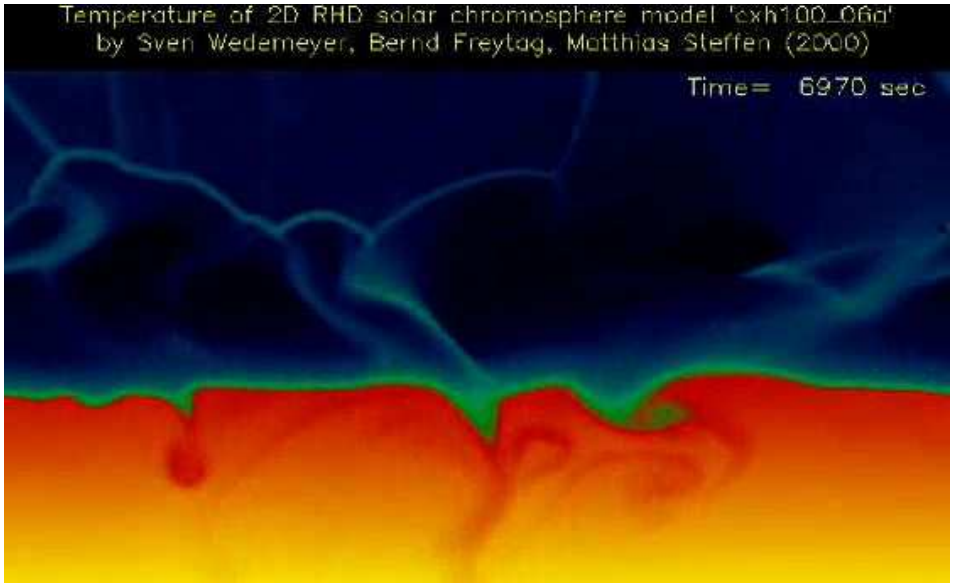

S. Wedemeyer et al. 2004, A&A 414, 1121

For a basic example of a shock capturing numerical scheme, consider a piecewise constant reconstruction with discontinuities at cell interfaces (S.K. Godunov, 1959).

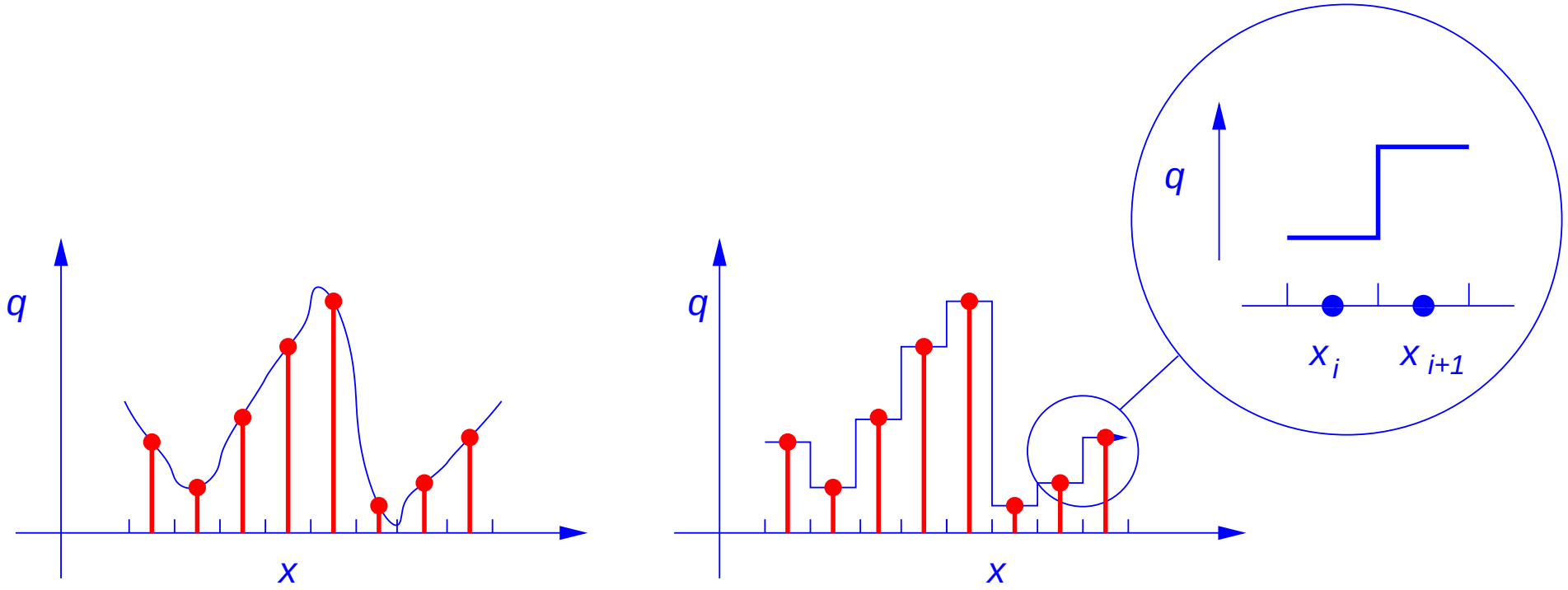

Solving the shock-tube problem for obtaining the fluxes at cell interfaces

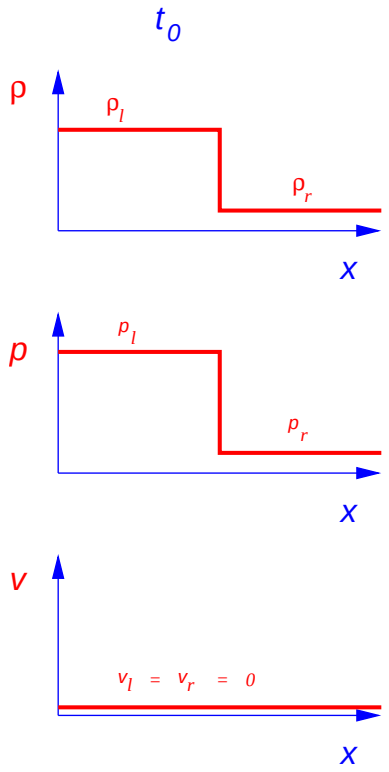

Solving the shock-tube problem for obtaining the fluxes at cell interfaces

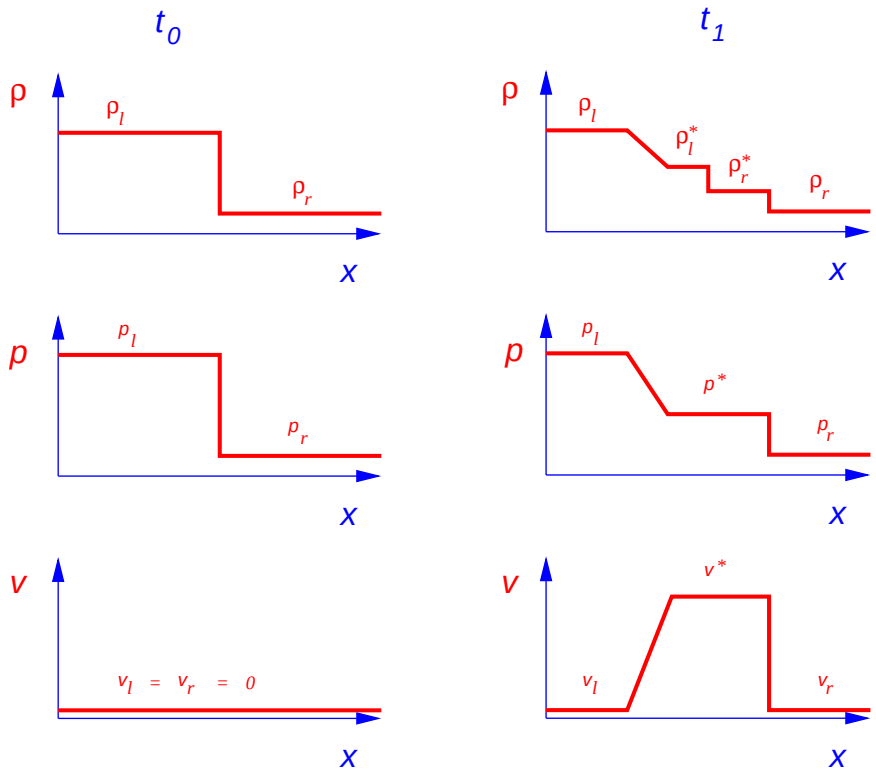

Solving the shock-tube problem for obtaining the fluxes at cell interfaces

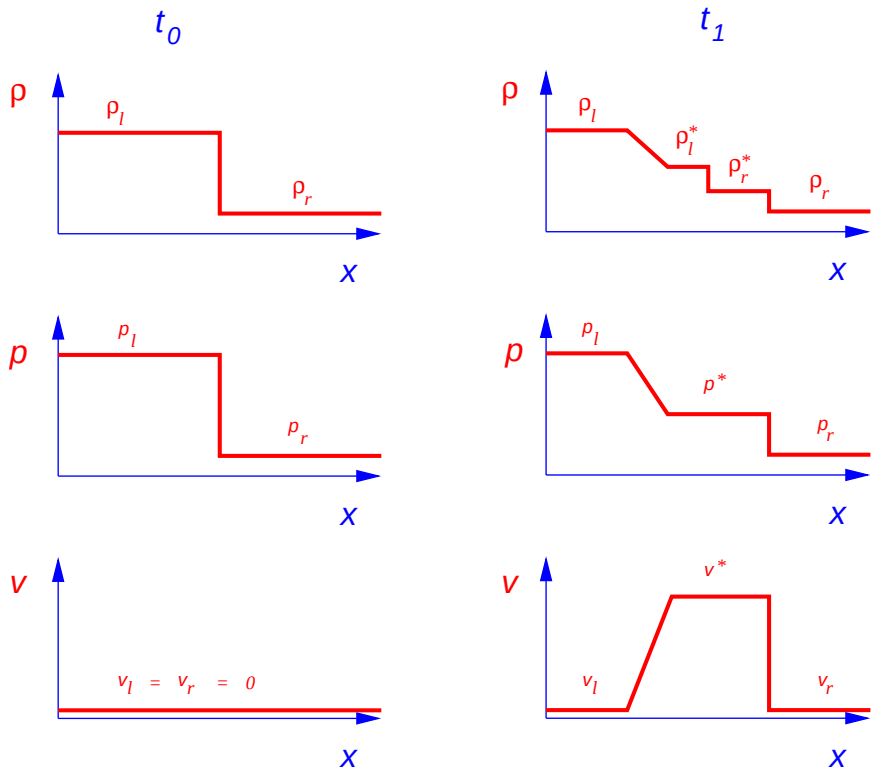

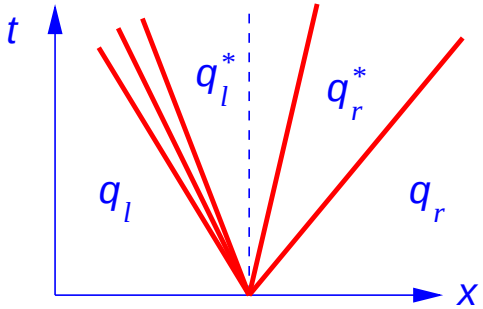

Solving the shock-tube problem for obtaining the fluxes at cell interfaces

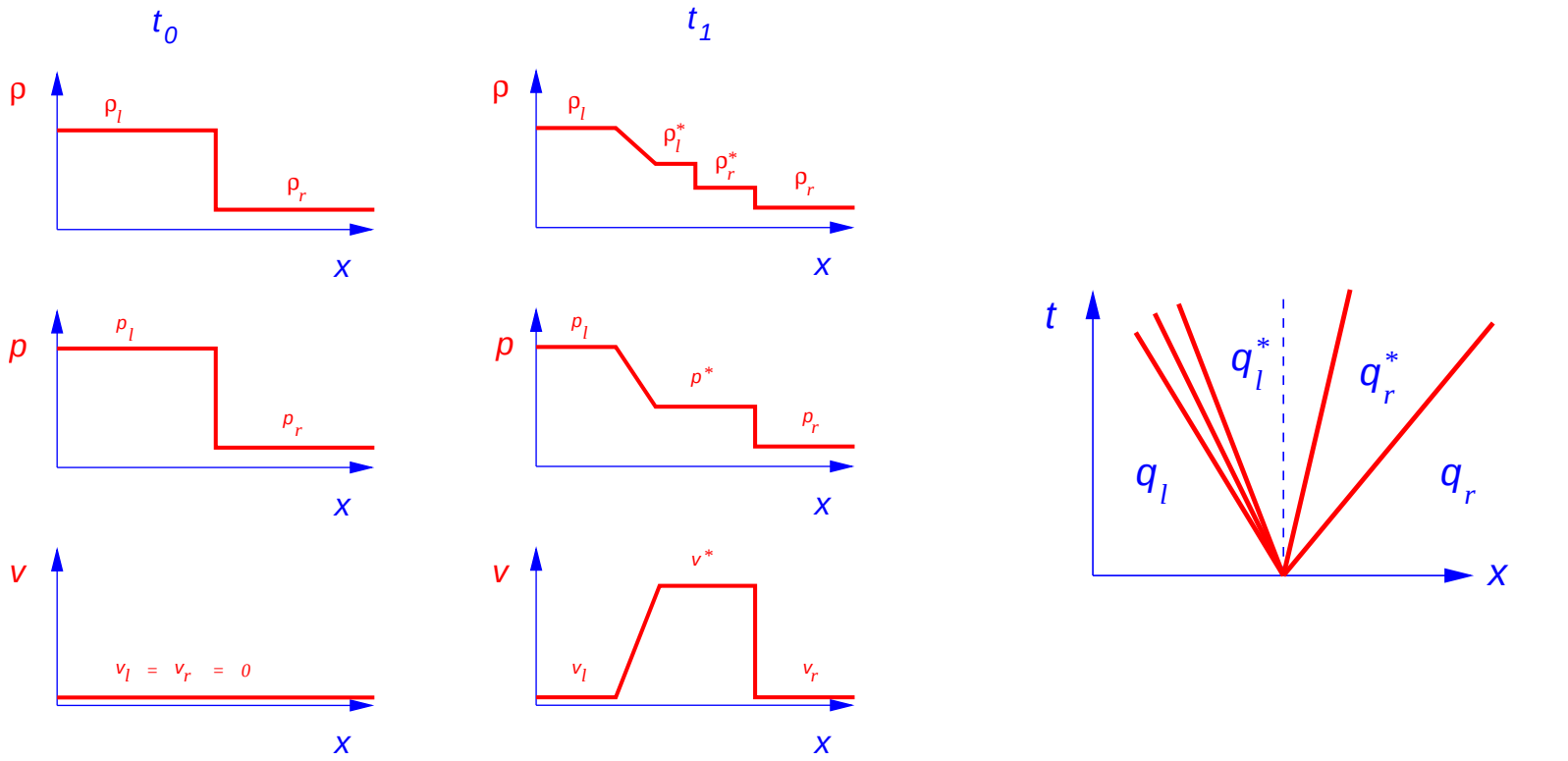

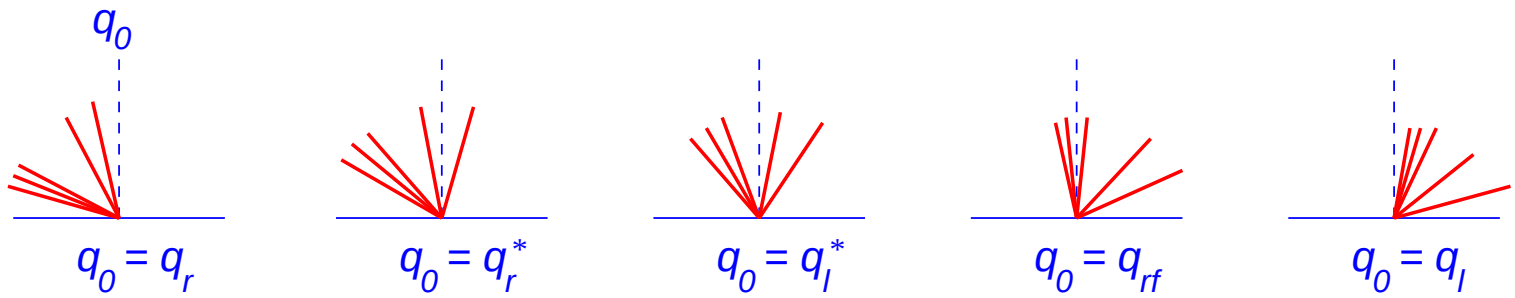

2.1. MHD-simulation from the convection zone to the chromosphere

The three-dimensional computational domain encompasses the integral layers from the upper convection zone to the middle chromosphere.

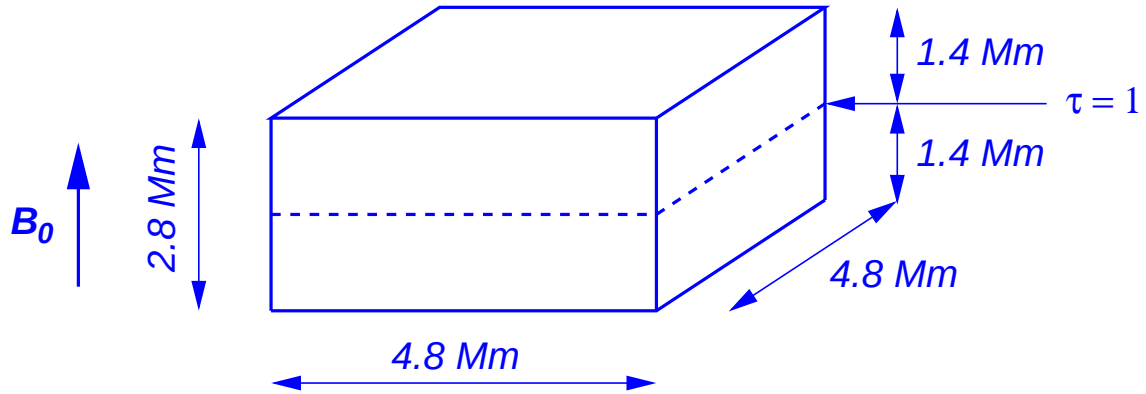

With 120^3 grid cells, the spatial resolution in the horizontal direction is 40 km, while in the vertical direction it is 20 km throughout the photosphere and chromosphere increasing to 50 km through the convection-zone layer.

MHD-simulation from the convection zone to the chromosphere (cont.)

The ideal MHD-equations can be written in conservative form as:

$$\frac{\partial \boldsymbol{U}}{\partial t} + \boldsymbol{\nabla} \cdot \boldsymbol{\mathcal{F}} = \boldsymbol{S} \,,$$

where the vector of conserved variables $\boldsymbol{U}$, the source term $\boldsymbol{S}$ due to gravity and radiation, and the flux tensor $\boldsymbol{\mathcal{F}}$ are

$$\boldsymbol{U} = (\rho, \rho\boldsymbol{v}, \boldsymbol{B}, E) \,, \qquad \boldsymbol{S} = (0, \rho\boldsymbol{g}, 0, \rho\boldsymbol{g} \cdot \boldsymbol{v} + q_{\mathrm{rad}}) \,,$$

$$\boldsymbol{\mathcal{F}} = \begin{pmatrix} \rho\boldsymbol{v} \\ \rho\boldsymbol{v}\boldsymbol{v} + \left(p + \frac{\boldsymbol{B}\cdot\boldsymbol{B}}{8\pi}\right)\boldsymbol{I} - \frac{\boldsymbol{B}\boldsymbol{B}}{4\pi} \\ \boldsymbol{v}\boldsymbol{B} - \boldsymbol{B}\boldsymbol{v} \\ \left(E + p + \frac{\boldsymbol{B}\cdot\boldsymbol{B}}{8\pi}\right)\boldsymbol{v} - \frac{1}{4\pi}\left(\boldsymbol{v}\cdot\boldsymbol{B}\right)\boldsymbol{B} \end{pmatrix} .$$

The tensor product of two vectors $\boldsymbol{a}$ and $\boldsymbol{b}$ is the tensor $\boldsymbol{a}\boldsymbol{b} = \boldsymbol{C}$ with elements $c_{mn} = a_m b_n$.

MHD-simulation from the convection zone to the chromosphere (cont.)

The total energy E is given by

$$E = \rho\epsilon + \rho\frac{\boldsymbol{v}\cdot\boldsymbol{v}}{2} + \frac{\boldsymbol{B}\cdot\boldsymbol{B}}{8\pi},$$

where ϵ is the thermal energy per unit mass. The additional solenoidality constraint,

$$\boldsymbol{\nabla}\cdot\boldsymbol{B} = 0,$$

must also be fulfilled. The MHD equations must be closed by an equation of state which gives the gas pressure as a function of the density and the thermal energy per unit mass

$$p = p(\rho, \epsilon)\,,$$

usually available to the program in tabulated form. The radiative source term is given by

$$q_{\rm rad} = 4\pi\rho\int\kappa_\nu(J_\nu - B_\nu)\mathrm{d}\nu\,,$$

$$J_\nu(\boldsymbol{r}) = \frac{1}{4\pi}\oint I_\nu(\boldsymbol{r},\boldsymbol{n})\mathrm{d}\Omega\,, \qquad I(\boldsymbol{r},\boldsymbol{n}) = I_0 e^{-\tau_0} + \int_0^{\tau_0}\left(\frac{\sigma}{\pi}T^4(\tau)\right)e^{-\tau}\mathrm{d}\tau$$

MHD-simulation from the convection zone to the chromosphere (cont.)

Common boundary conditions for the thermal variables and velocities

$$\frac{\partial v_{x,y}}{\partial z} = 0\,;\; v_z = 0\,;\; \frac{\partial \epsilon}{\partial z} = 0 \quad \text{or} \quad \frac{\partial^2 \epsilon}{\partial z^2} = 0$$

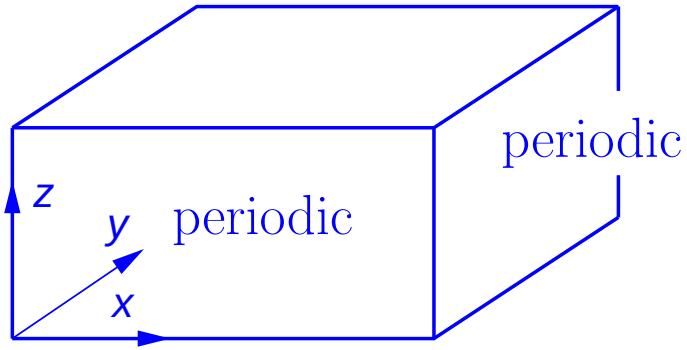

$$\frac{\partial v_{x,y}}{\partial z} = 0\,;\; \int \rho v_z \,\mathrm{d}\sigma = 0\,;\; \text{outflow: } \frac{\partial s}{\partial z} = 0$$

$$\text{inflow: } s = \text{const}$$

Both runs have *periodic lateral boundary conditions* in all variables. *Open bottom boundary* in the sense that the fluid can freely flow in and out of the computational domain under the condition of vanishing total mass flux.

Reflecting (closed) top boundary in run v10. Open top boundary in run h20.

MHD-simulation from the convection zone to the chromosphere (cont.)

Different boundary conditions for the magnetic field

v10

$B_{x,y} = 0\,;\ \frac{\partial B_z}{\partial z} = 0$

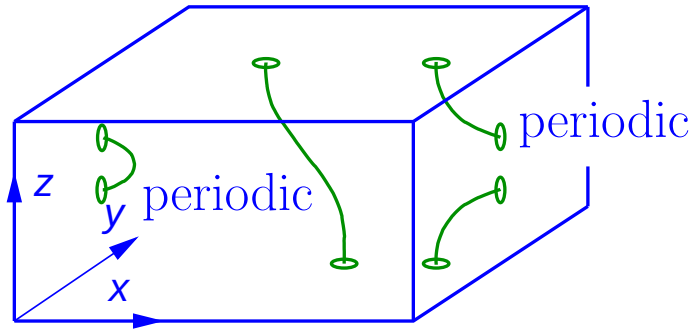

$B_{x,y} = 0\,;\ \frac{\partial B_z}{\partial z} = 0$

h20

$\frac{\partial B_{x,y,z}}{\partial z} = 0$

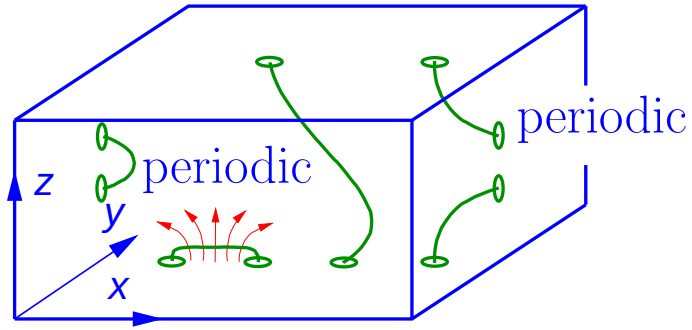

outflow: $\frac{\partial B_{x,y,z}}{\partial z} = 0$

inflow: $B_y = B_z = 0, B_x = \text{const.}$

$B_x = 20$ G

Different initial states for the magnetic field

v10

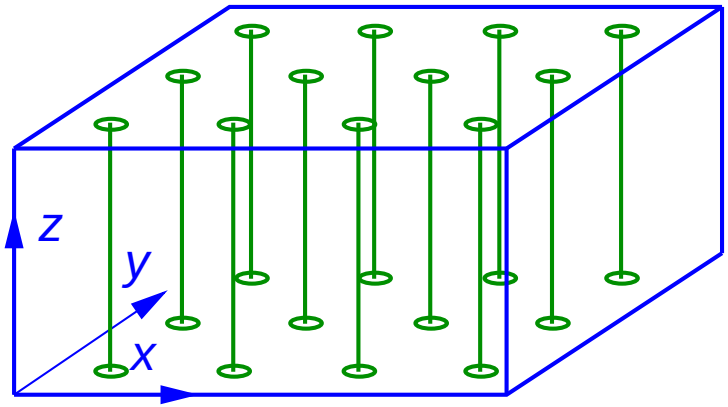

Initial homogeneous, vertical, unipolar **B**-field of 10 G.

h20

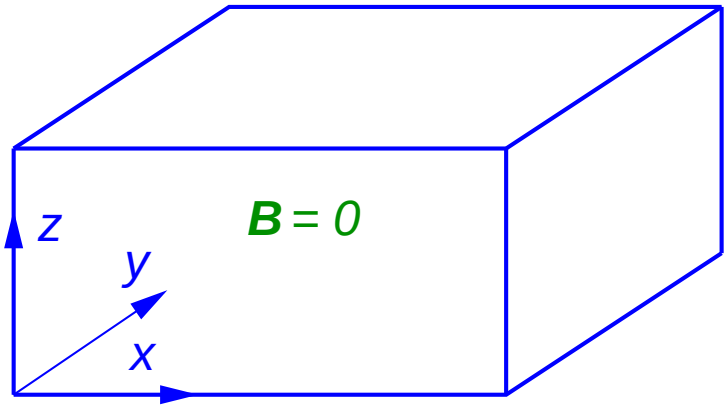

Fluid that enters the simulation domain from below carries horizontal magnetic field of a uniform flux density of 20 G and of uniform direction parallel to the x-axis

MHD-simulation from the convection zone to the chromosphere (cont.)

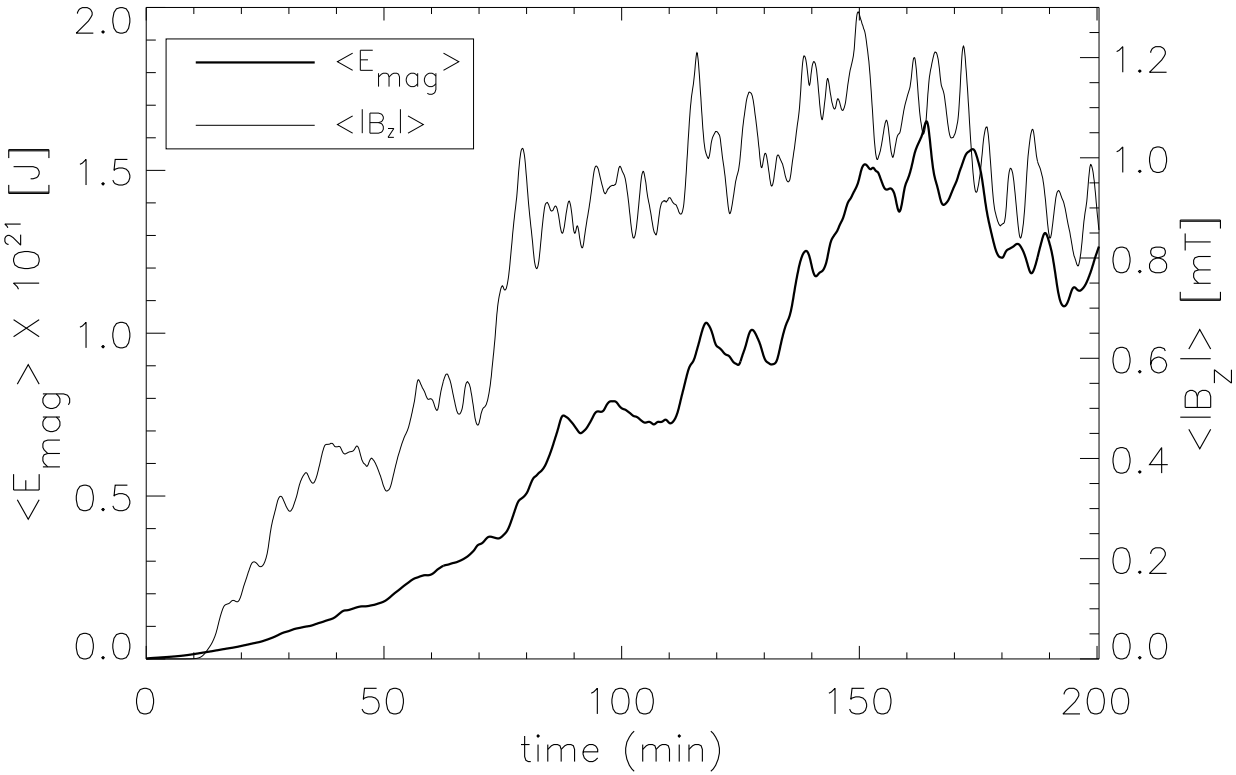

Growth of magnetic energy in the computational box of *run h20* and mean absolute vertical magnetic field strength at a fixed geometrical height corresponding to the mean optical depth unity, $\langle |B_z| \rangle (\langle \tau_{500\,\mathrm{nm}} \rangle = 1)$.

MHD-simulation from the convection zone to the chromosphere (cont.)

Vertical cross sections through 3-D simulation domain

v10

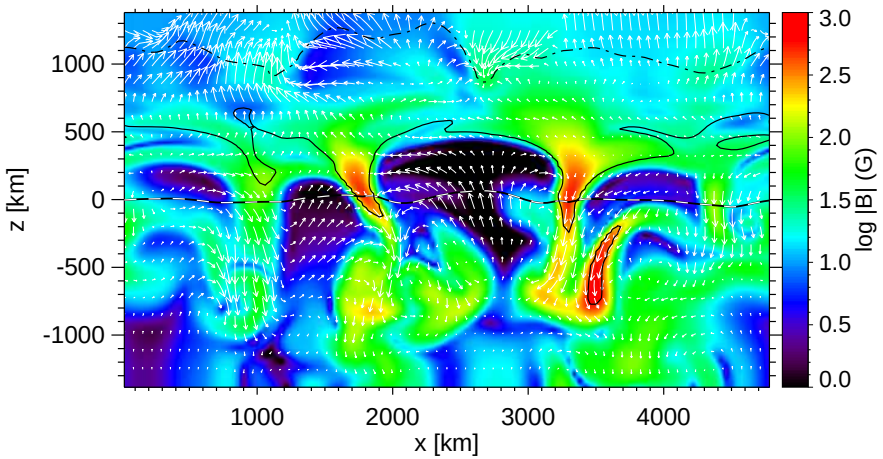

Colors indicate $0 \leq \log |B| \leq 3.0$

h20

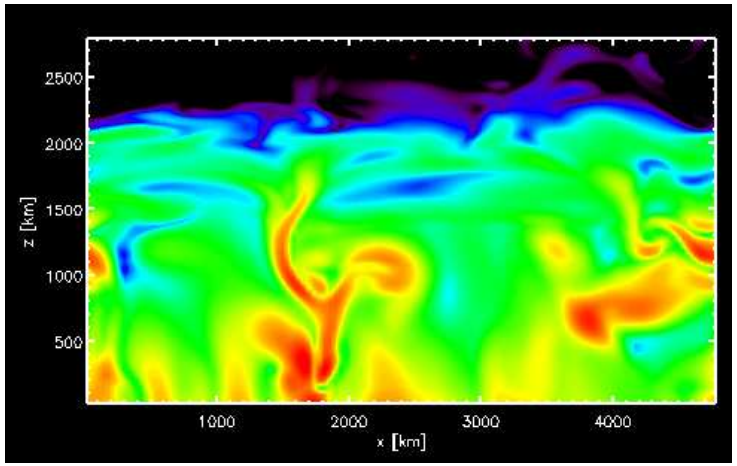

Colors indicate $0.5 \leq \log |B| \leq 2.5$

3. Structure and development of the horizontal magnetic field

Horizontally and temporally averaged absolute vertical and horizontal magnetic flux density as a function of height for both runs.

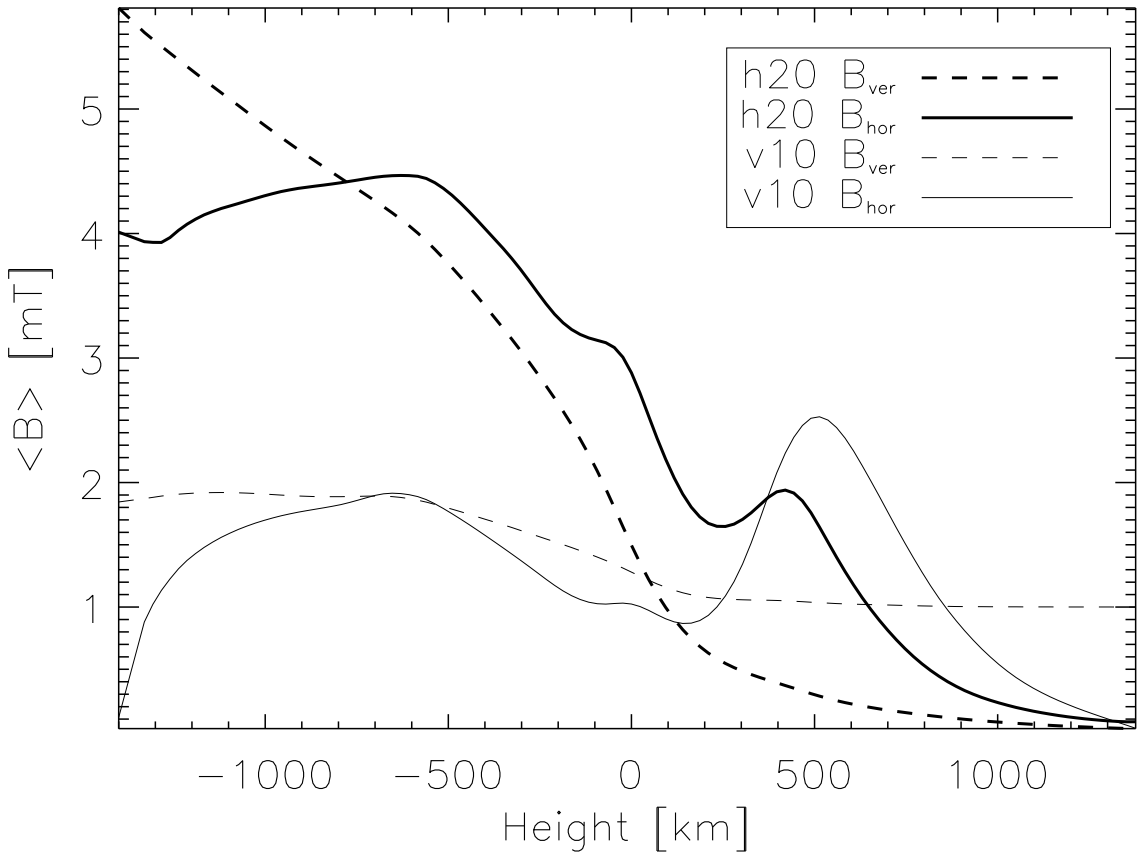

run v10:

$\langle |B_{\rm hor}| \rangle / \langle |B_{\rm ver}| \rangle (350\,\text{km}) = 2.5$

run h20:

$\langle |B_{\rm hor}| \rangle / \langle |B_{\rm ver}| \rangle (250\,\text{km}) = 5.6$

Structure and development of the horizontal magnetic field (cont.)

Snapshot of $B_{\rm hor}$ and $B_{\rm ver}$ of *run h20* in the horizontal section of $\langle \tau_{500\,\rm nm} \rangle = 1$.

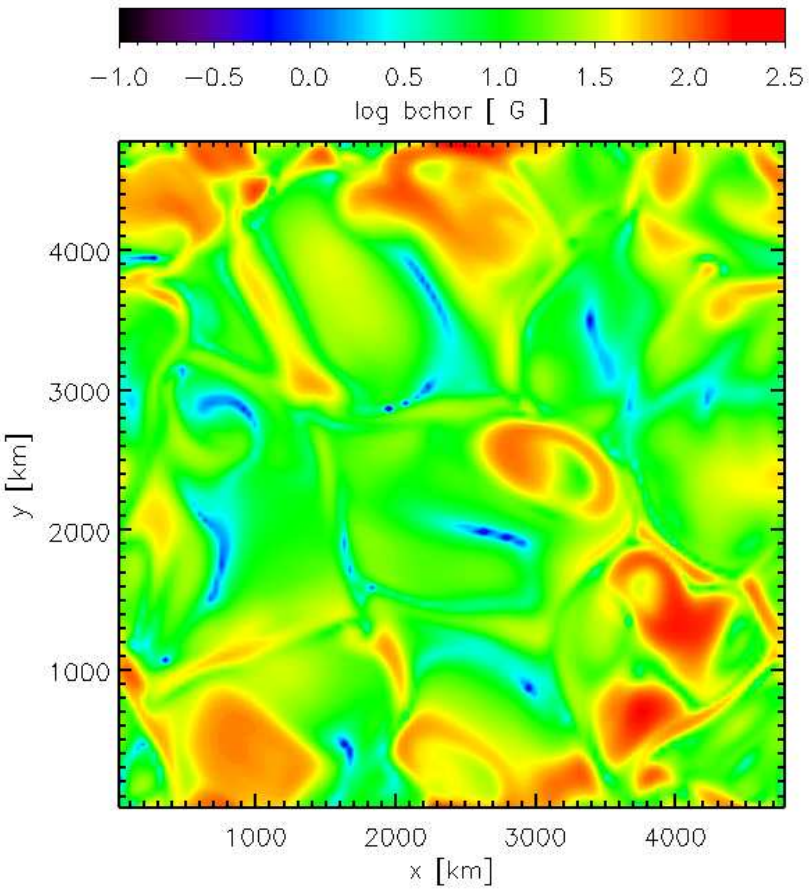

$B_{\rm hor}$

areal fraction with $B_{\rm hor} > 5$ mT $= 17\%$

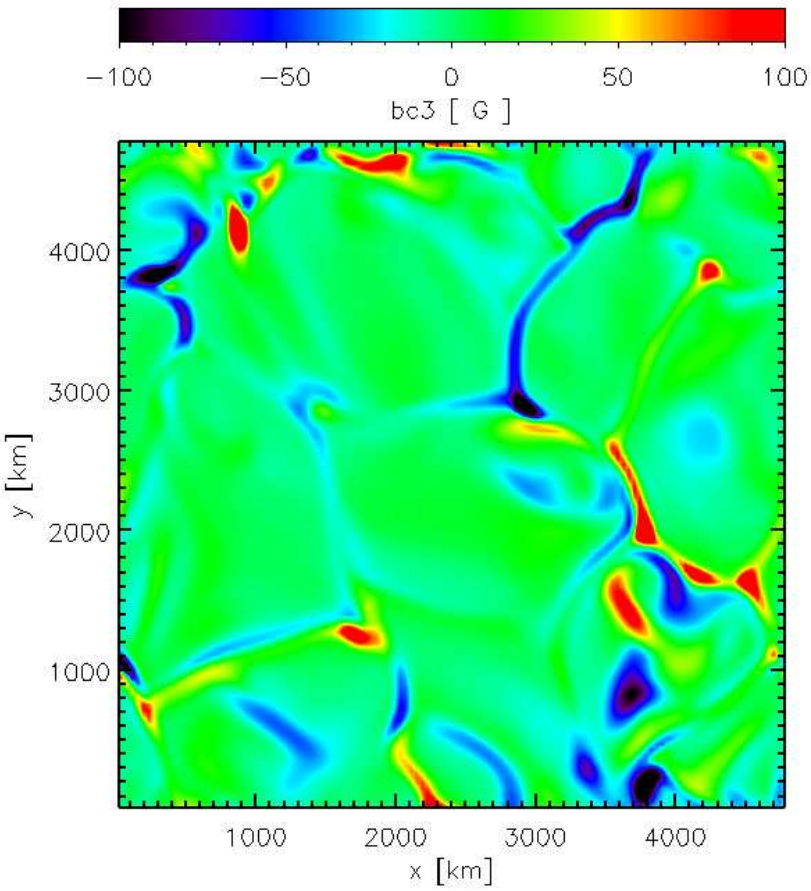

$B_{\rm ver}$

areal fraction with $B_{\rm ver} > 5$ mT $= 2.2\%$

Structure and development of the horizontal magnetic field (cont.)

Vertically directed Poynting flux, $\langle S_z \rangle$, $\langle B_{\rm hor} \rangle$, and $\langle |B_z| \rangle$ as a function of time and height in the atmosphere.

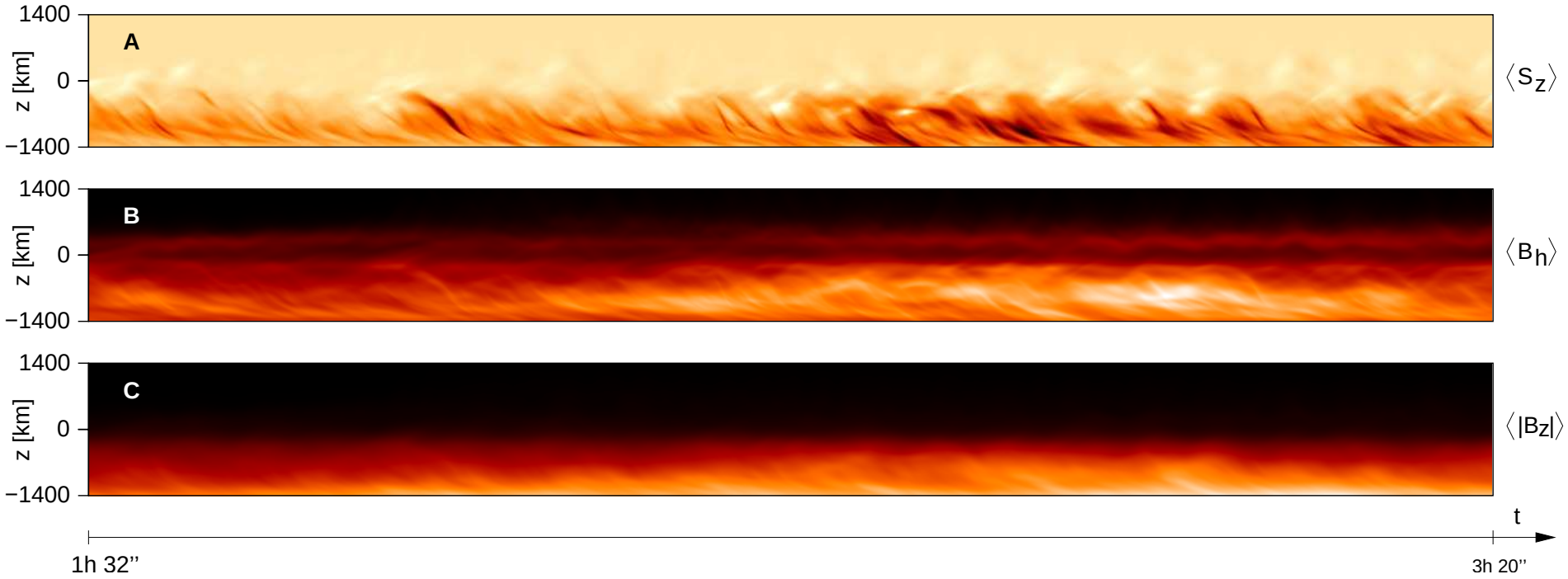

The surface of optical depth unity acts as a separatrix for the vertically directed Poynting flux.

$$\mathbf{S} = \frac{1}{4\pi}(\mathbf{B} \times (\mathbf{v} \times \mathbf{B}))$$

Structure and development of the horizontal magnetic field (cont.)

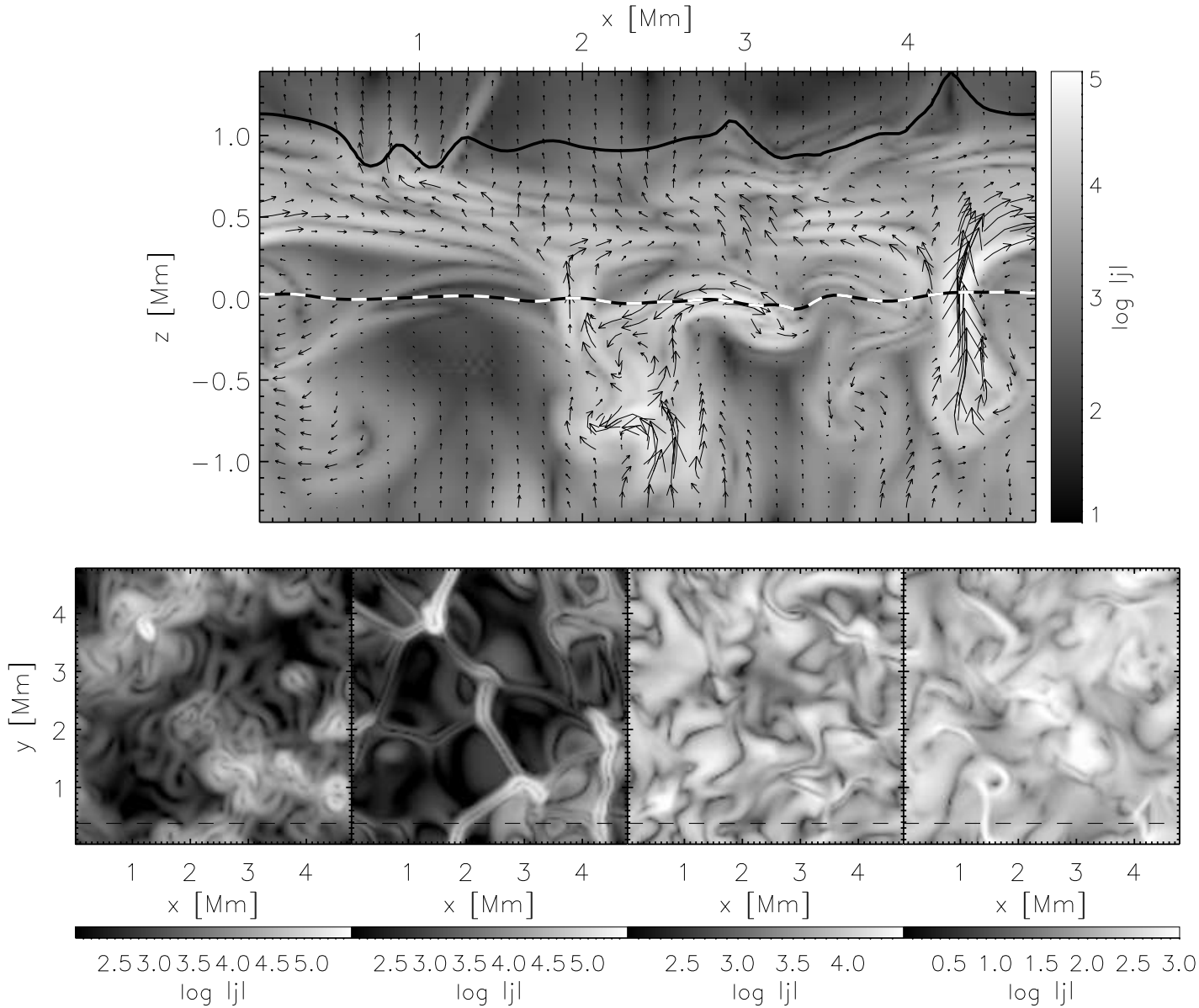

Logarithmic current density, $\log |j|$, in a vertical cross section (top panel) and in four horizontal cross sections in a depth of 1180 km below, and at heights of 90 km, 610 km, and 1310 km above the average height of optical depth unity from left to right, respectively. The arrows in the top panel indicate the *magnetic field* strength and direction.

From Schaffenberger, Wedemeyer-Böhm, Steiner, and Freytag, 2006, ASP Conf. Ser., Vol. 354, p. 345

3.1. Comparison with polarimetry from Hinode

Lites et al. (2007) found from the deep mode series

$$\frac{\langle B^{\rm T}_{\rm app}\rangle}{\langle B^{\rm L}_{\rm app}\rangle} = \frac{55.3\,\mathrm{Mx\,cm^{-2}}}{11.0\,\mathrm{Mx\,cm^{-2}}} \approx 5\ .$$

From the simulation we find

$$\frac{\langle B_{\rm hor}\rangle}{\langle |B_{\rm ver}|\rangle} = \begin{cases} 25\,\mathrm{G}/10.2\,\mathrm{G} = 2.5 & \text{for run } \textit{v10} \\ 19.5\,\mathrm{G}/3.8\,\mathrm{G} = 5.6 & \text{for run } \textit{h20} \end{cases}\ .$$

But remember the difference between apparent and true magnetic flux density!

Comparison with polarimetry from Hinode (cont.)

From the two simulation runs, we synthesized the Stokes profiles of both 630 nm Fe I spectral lines observed by the Hinode SP. Profiles were computed with the radiative transfer code SIR along vertical lines of sight (disk center) with a spectral sampling of 2 pm.

$I_{630\,\mathrm{nm}}$

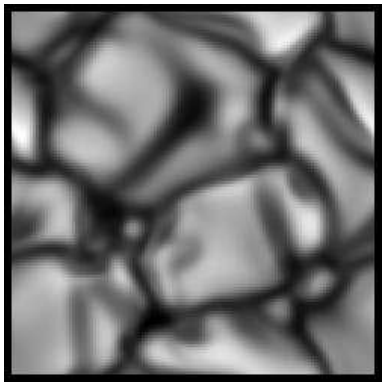

$V_{\mathrm{tot}\,630\,\mathrm{nm}}$

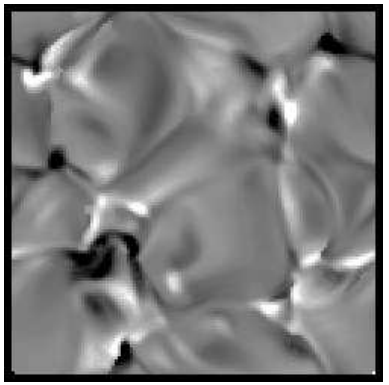

For a faithful comparison with the results of Lites et al. we subject the synthetic profiles to exactly the same procedure for conversion to apparent flux density as was done with the real data.

Comparison with polarimetry from Hinode (cont.)

The conversion to apparent flux densities proceeds by *first* computing

$$V_{\rm tot} = \text{sign}(V_{\rm blue}) \frac{|\int_0^{\lambda_0} V(\lambda){\rm d}\lambda| + |\int_{\lambda_0}^{\infty} V(\lambda){\rm d}\lambda|}{I_c \int {\rm d}\lambda} \ ,$$

and

$$Q_{\rm tot} = \frac{\int Q(\lambda) Q_{\rm mask}(\lambda){\rm d}\lambda}{I_c \int Q_{\rm mask}(\lambda){\rm d}\lambda} \ ,$$

where Q is mesured relative to the "preferred-frame azimuth" ϕ_r, viz, relative to the projection of the magnetic field vector on the plane of sky. $Q_{\rm mask}$ is a weightening factor that is the normalized sum of all the Q-profiles in the preferred-frame azimuth.

Second, we compute $V_{\rm tot}$ and $Q_{\rm tot}$ for a standard atmosphere with a given (known) set of homogeneous magnetic fields for establishing a *calibration curve*.

Comparison with polarimetry from Hinode (cont.)

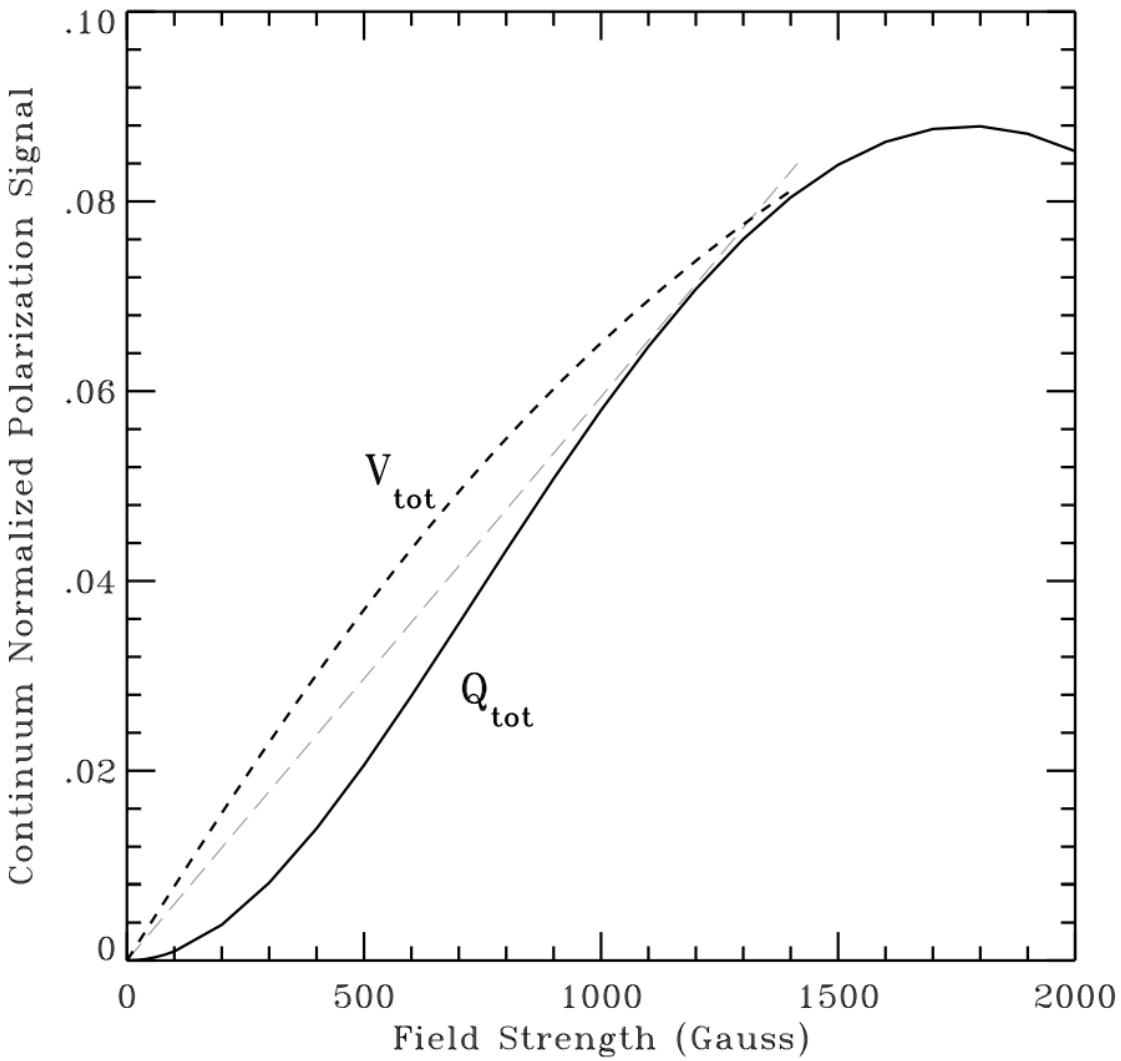

Calibration curve from Lites et al. 07 derived from a Milne-Eddington atmosphere with a homogeneous horizontal magnetic field for $Q_{\rm tot}$ and a magnetic field inclined by 45° for $V_{\rm tot}$.

Comparison with polarimetry from Hinode (cont.)

Lites et al. (2007) found from the deep mode series

$$\frac{\langle B^{\rm T}_{\rm app}\rangle}{\langle B^{\rm L}_{\rm app}\rangle} = \frac{55.3\,\mathrm{Mx\,cm^{-2}}}{11.0\,\mathrm{Mx\,cm^{-2}}} \approx 5\ .$$

From the simulation we find

$$\frac{\langle B_{\rm hor}\rangle}{\langle |B_{\rm ver}|\rangle} = \begin{cases} 25\,\mathrm{G}/10.2\,\mathrm{G} = 2.5 & \text{for run } \textit{v10} \\ 19.5\,\mathrm{G}/3.8\,\mathrm{G} = 5.6 & \text{for run } \textit{h20} \end{cases}\ .$$

From the synthesized Fe I 630 nm Stokes profile pair we find

$$\frac{\langle B^{\rm T}_{\rm app}\rangle}{\langle B^{\rm L}_{\rm app}\rangle} = \begin{cases} 11.5\,\mathrm{G}/7.5\,\mathrm{G} = 1.5 & \text{for run } \textit{v10} \\ 24.8\,\mathrm{G}/8.8\,\mathrm{G} = 2.8 & \text{for run } \textit{h20} \end{cases}\ .$$

4. The structure of internetwork magnetic elements

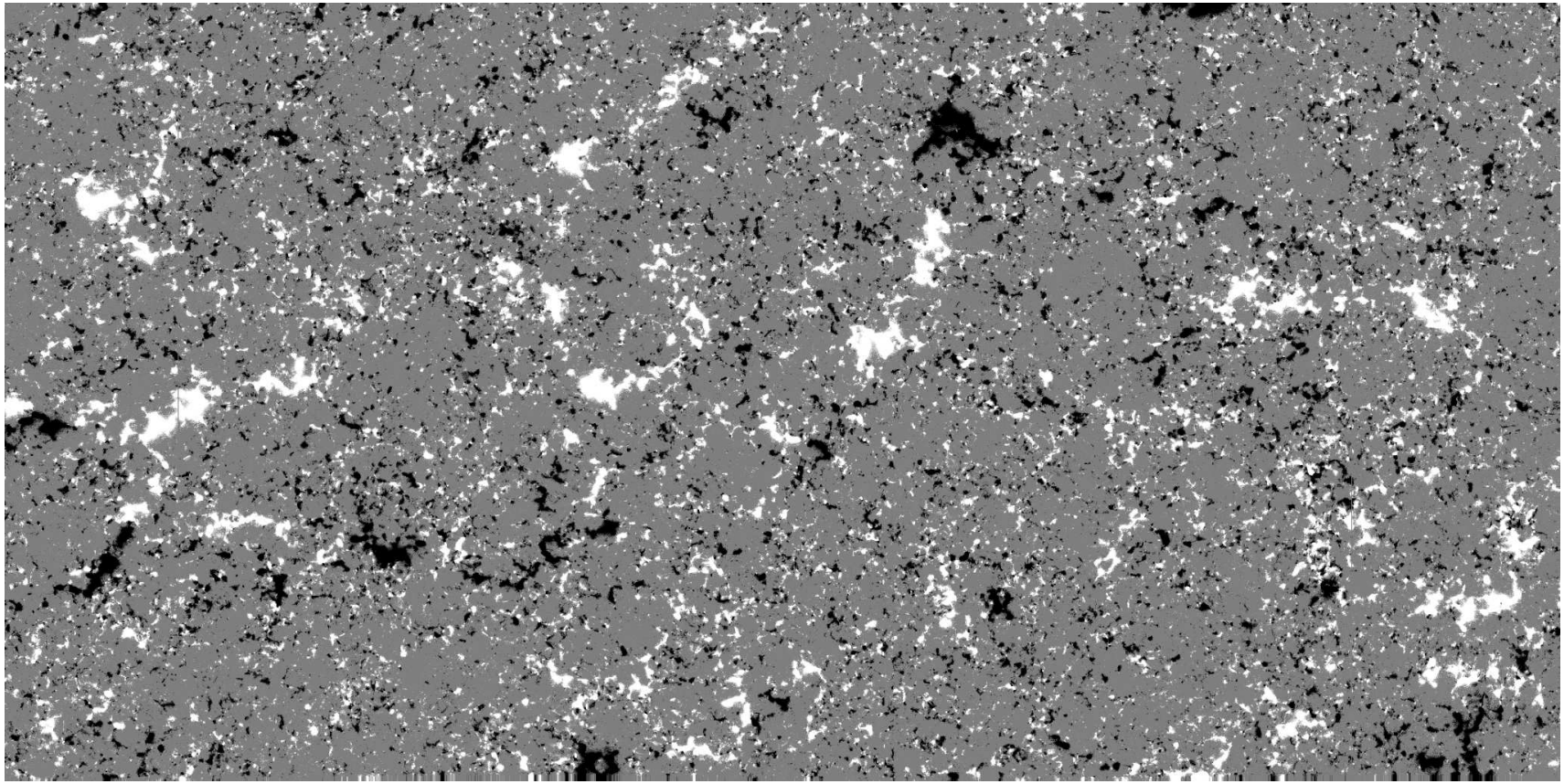

Apparent vertical magnetic flux density $B^{\mathrm{L}}_{\mathrm{app}}$ of the quiet Sun over a field of view of $302'' \times 162''$ observed from the Hinode space observatory. The grey scale saturates at ± 50 Mx cm^{-2}. 2048 steps to 5 s.

The structure of internetwork magnetic elements (cont.)

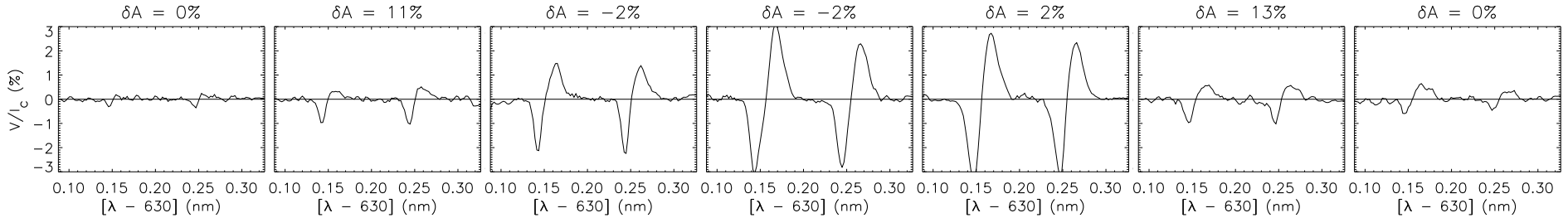

Stokes-V profiles across a magnetic element of the internetwork from the Hinode data.

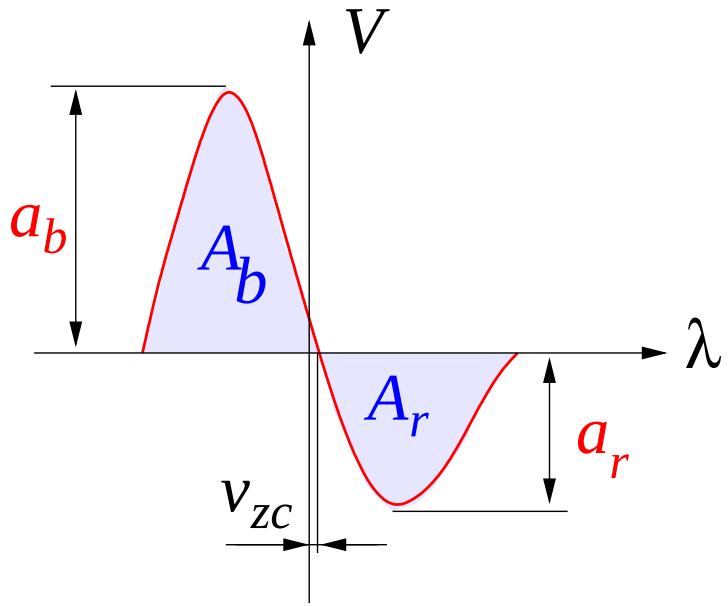

$$\delta A := \frac{A_b - A_r}{A_b + A_r}$$

$$\text{sign}(\delta A) = -\text{sign}\left(\frac{\mathrm{d}|B|}{\mathrm{d}\tau} \cdot \frac{\mathrm{d}v(\tau)}{\mathrm{d}\tau}\right)$$

Solanki & Pahlke, 1988; Sanchez Almeida et al., 1989

The structure of internetwork magnetic elements (cont.)

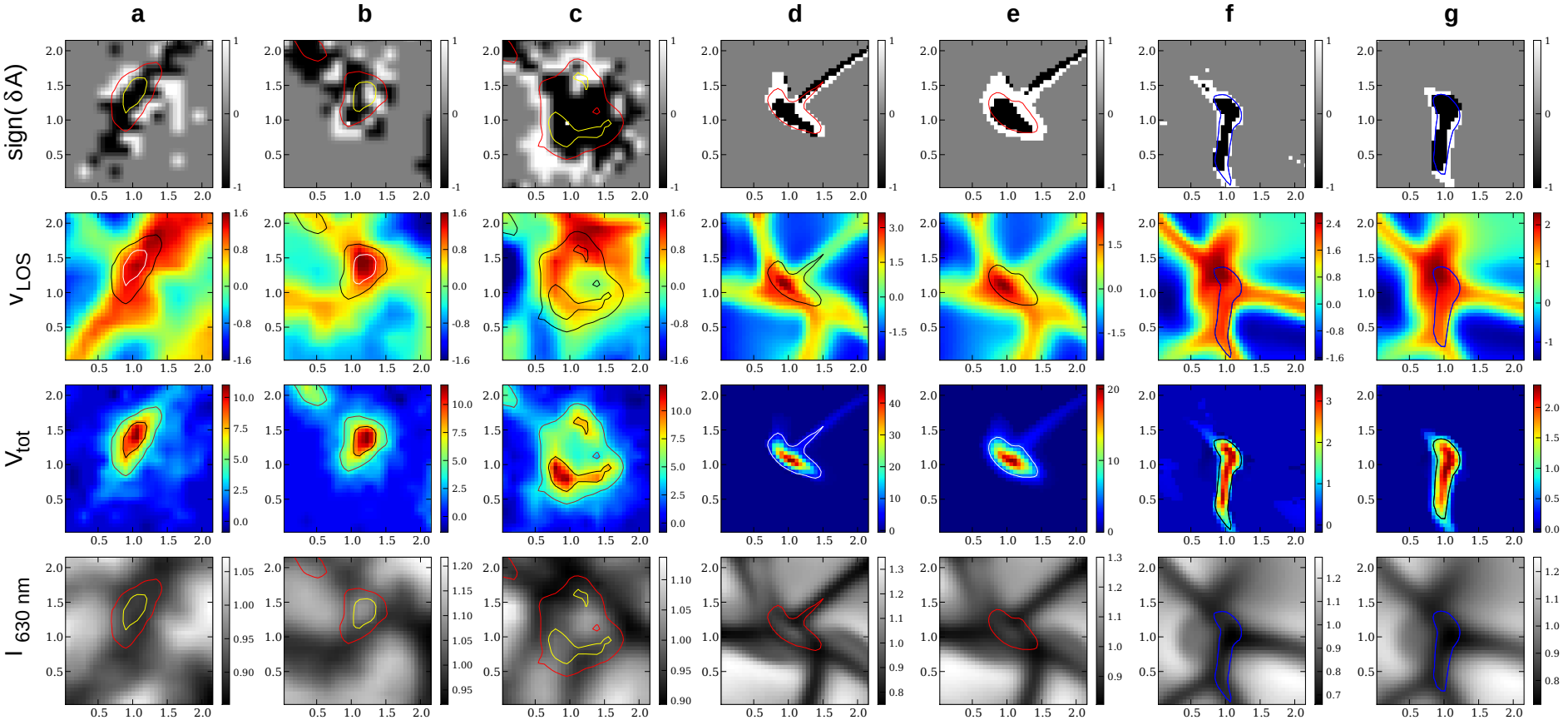

Columns a-c: observational data obtained with the spectro-polarimeter of Hinode/SOT. *Columns d and f*: synthetic data from the 3-D MHD simulation. *Columns e and g*: same as d and f but after application of the SOT-PSF to the synthetic intensity maps. Distance between tick marks is $0.5''$.

From *Rezaei, Steiner, Wedemeyer-Böhm et al. 2007, A&A 476, L33*

The structure of internetwork magnetic elements (cont.)

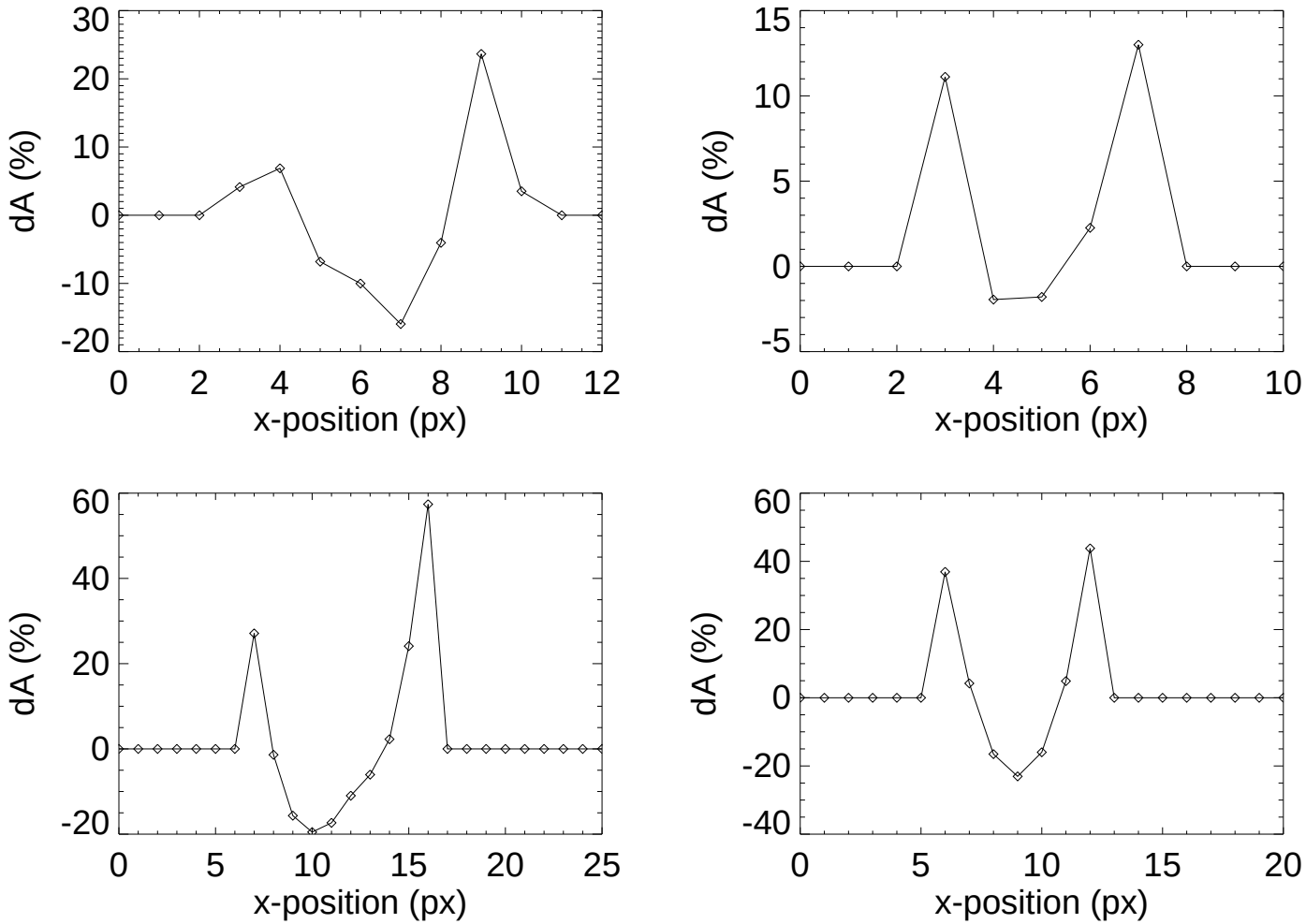

Variation in δA across magnetic elements from the Hinode data *(top row)* and the simulation *(bottom row)*.

The structure of internetwork magnetic elements (cont.)

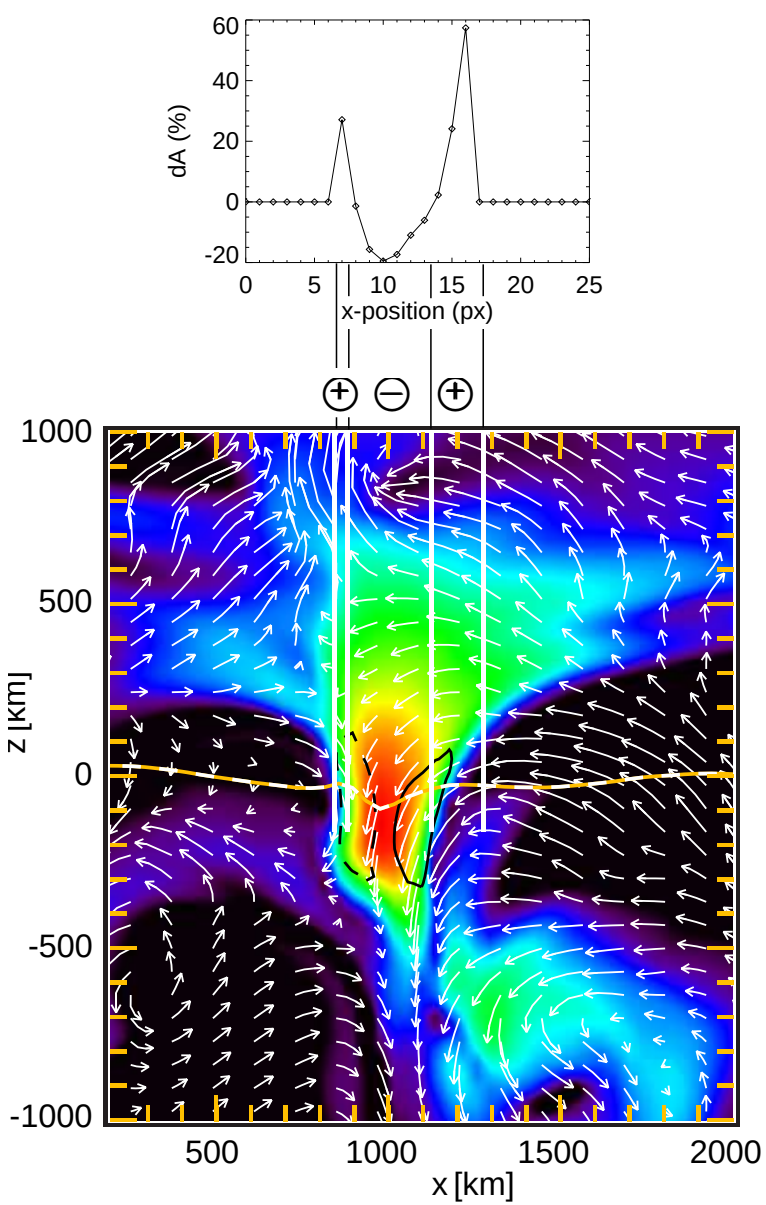

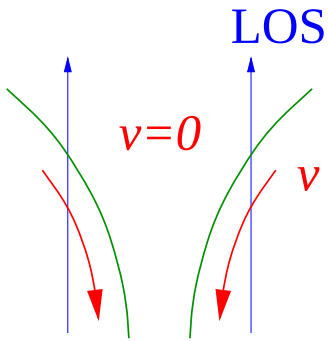

$$\left.\begin{array}{l} \frac{\mathrm{d}|B|}{\mathrm{d}\tau} < 0 \\ \frac{\mathrm{d}v(\tau)}{\mathrm{d}\tau} > 0 \end{array}\right\} \Rightarrow \delta A > 0$$

Vertical cross section through the simulation box. *Colour* displays the logarithmic magnetic field strength, *arrows* the velocity field, *black contours* the electric current density normal to the plane. The *white vertical lines* indicate ranges of either positive or negative area asymmetry, δA.

5. The magnetic field of the internetwork chromosphere

Synoptic summary of magnetoconvective simulation from the convection zone to the chromosphere.

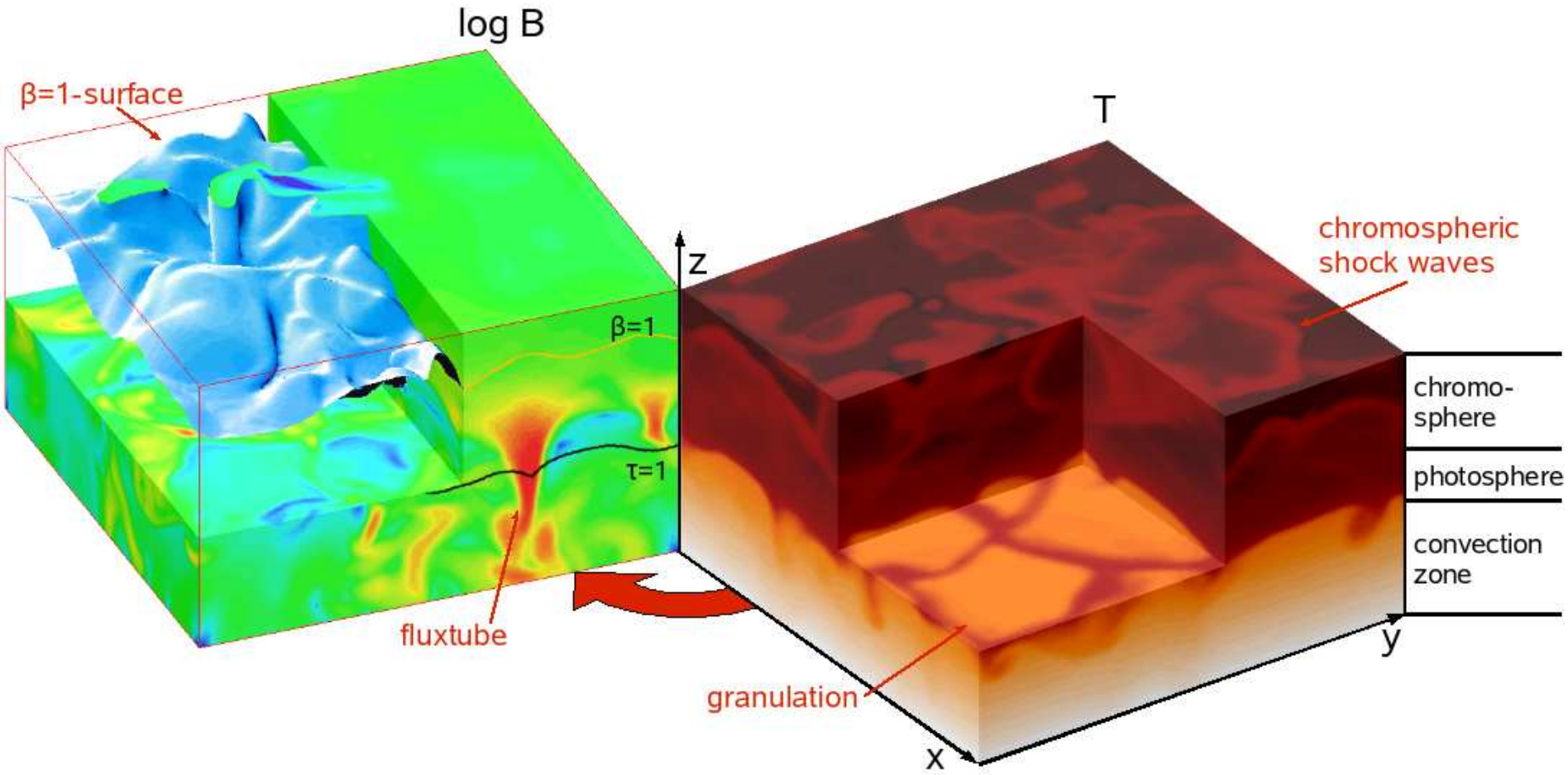

The magnetic field of the internetwork chromosphere (cont.)

Case v10: boundary and initial conditions for the magnetic field

v10

$$B_{x,y} = 0\,;\ \frac{\partial B_z}{\partial z} = 0$$

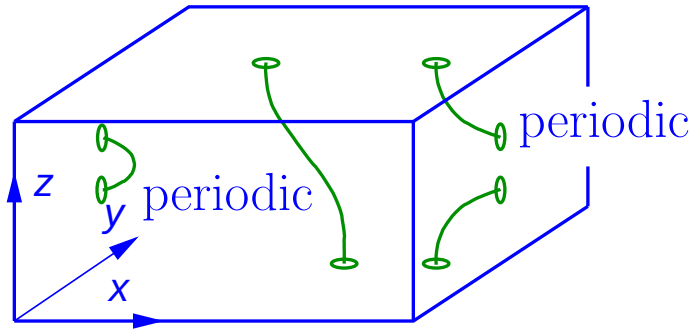

$$B_{x,y} = 0\,;\ \frac{\partial B_z}{\partial z} = 0$$

v10

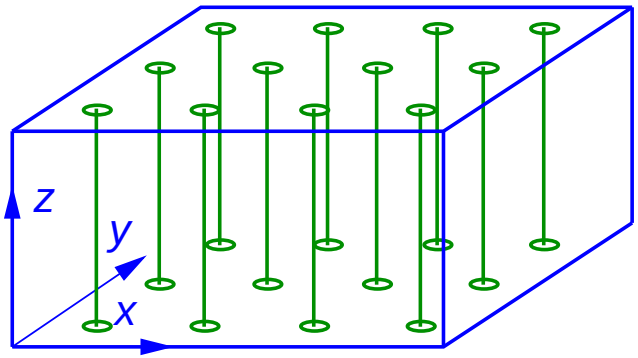

Initial homogeneous, vertical, unipolar

B-field of 10 G.

The magnetic field of the internetwork chromosphere (cont.)

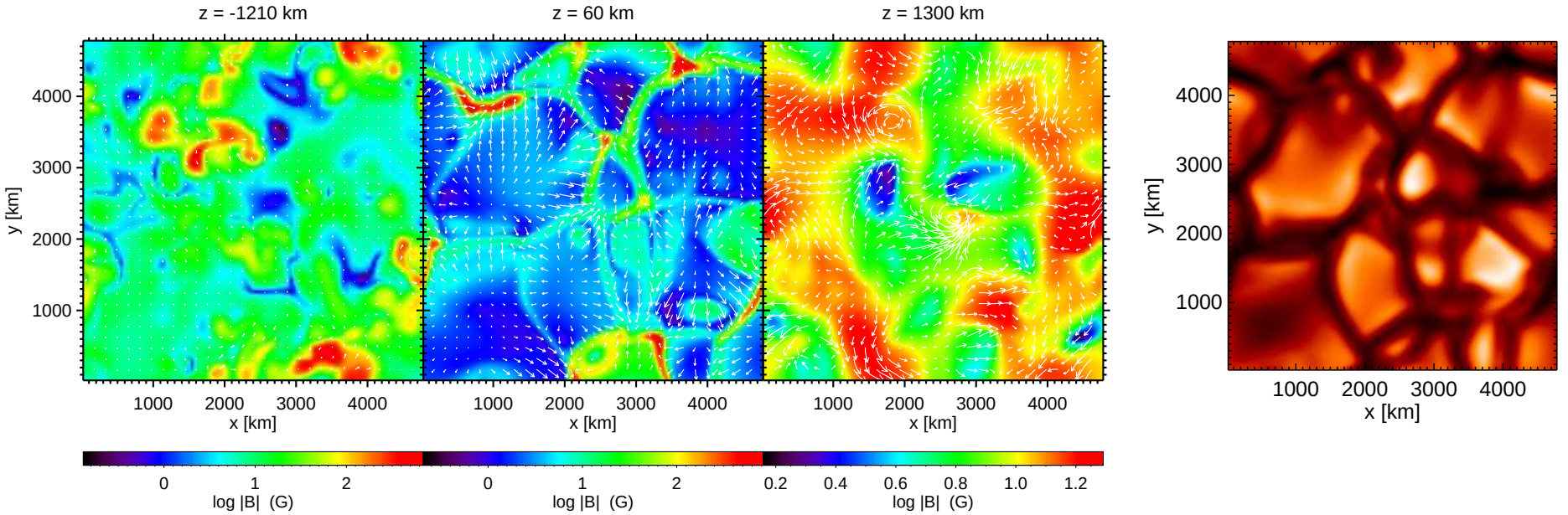

Horizontal sections through 3-D computational domain. Color coding displays $\log |B|$ with individual scaling for each panel. **Left:** Bottom layer at a depth of 1210 km. **Middle:** Layer 60 km above optical depth $\tau_c = 1$. **Right:** Top, chromospheric layer in a height of 1300 km. White arrows indicate the horizontal *velocity* on a common scaling. Longest arrows in the panels from left to right correspond to 4.5, 8.8, and 25.2 km/s, respectively. **Rightmost:** Emergent *intensity*.

The magnetic field of the internetwork chromosphere (cont.)

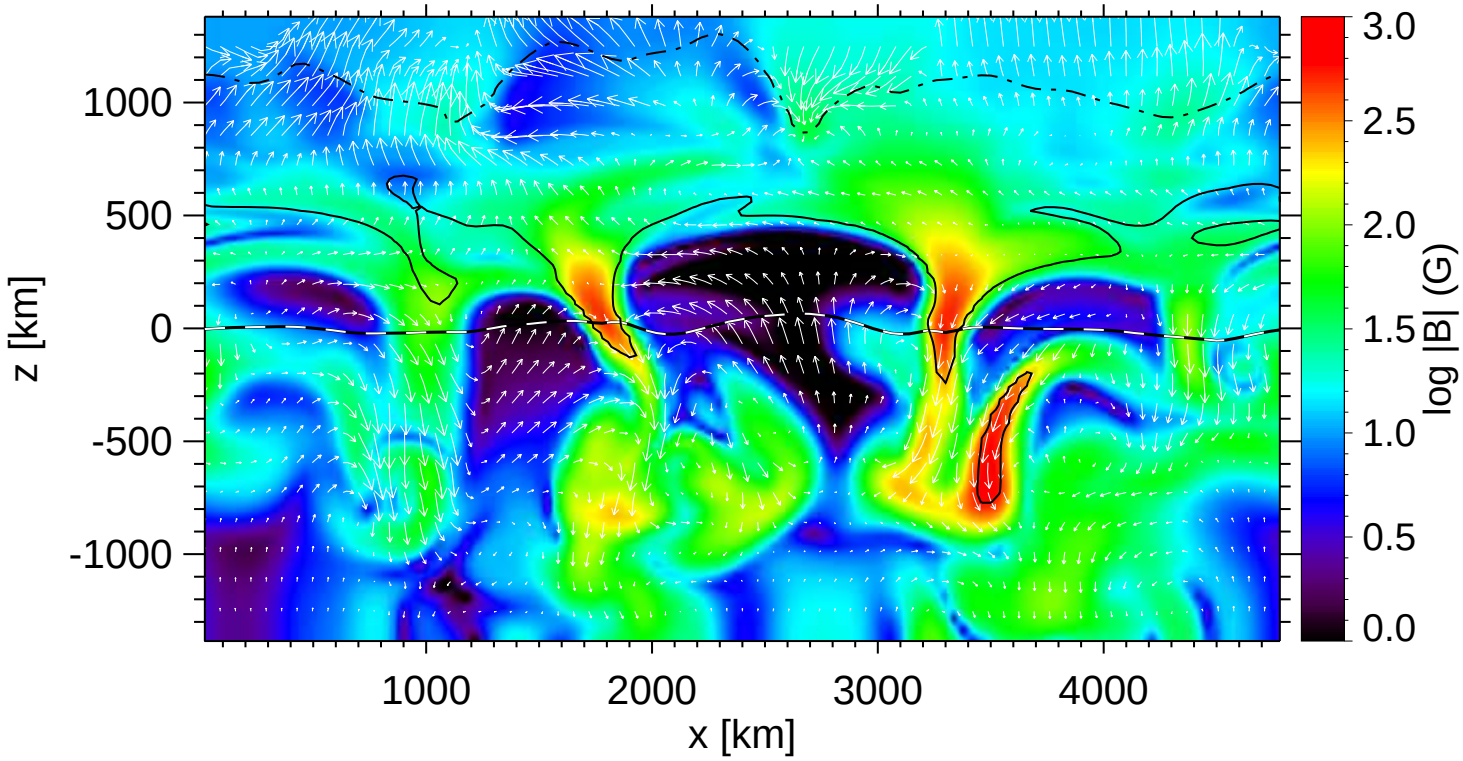

Snapshot of a vertical section showing $\log|B|$ (color coded) and *velocity vectors* projected on the vertical plane (white arrows). The b/w dashed curve shows optical depth unity and the dot-dashed and solid black contours $\beta = 1$ and 100, respectively. movie with $\beta = 1$ surface

Schaffenberger, Wedemeyer-Böhm, Steiner & Freytag, 2005, in *Chromospheric and Coronal Magnetic Fields*, Innes, Lagg, Solanki, & Danesy (eds.), ESA Publication SP-596

The magnetic field of the internetwork chromosphere (cont.)

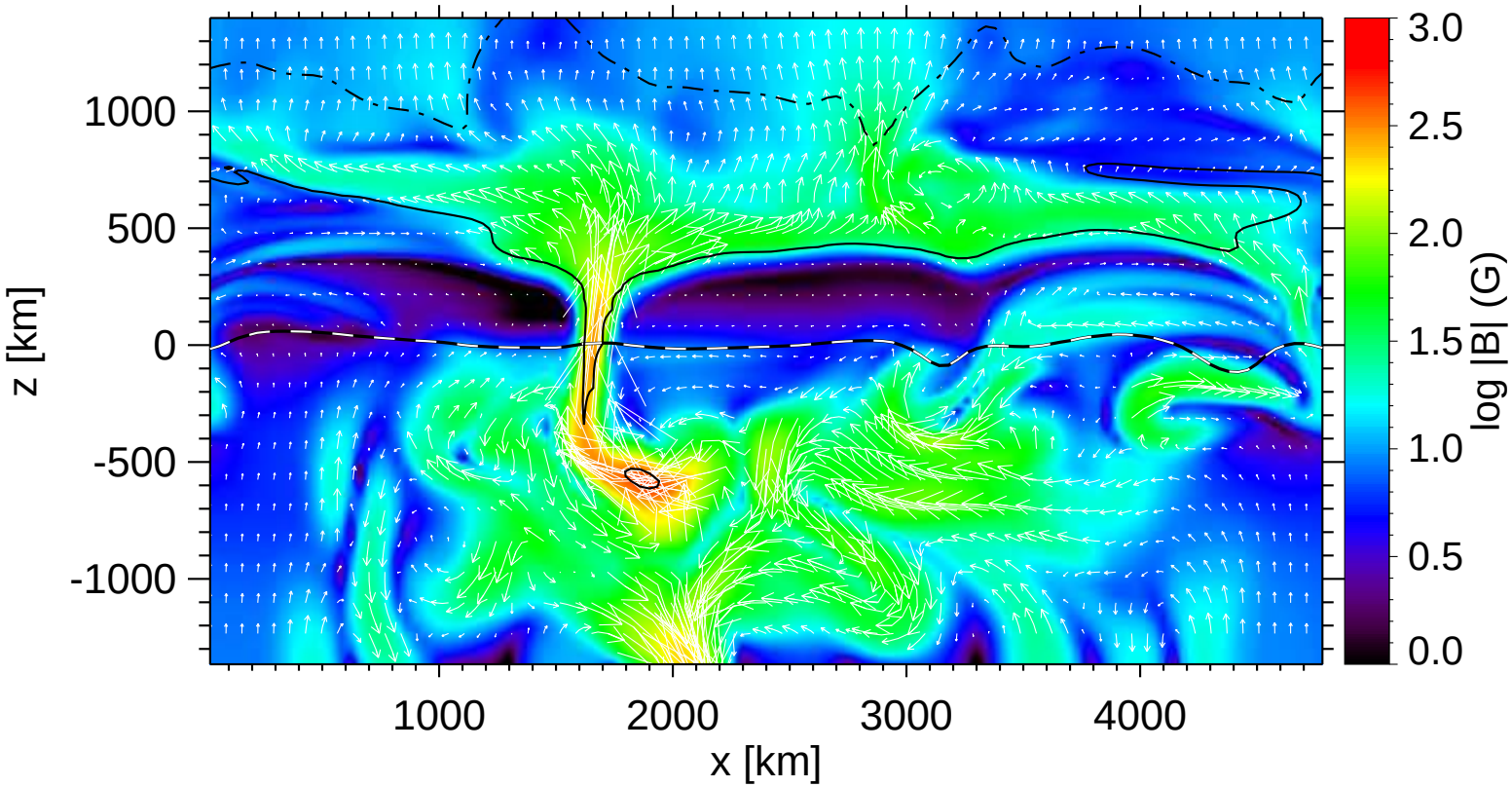

Snapshot of a vertical section showing $\log|B|$ (color coded) and $\mathbf{B}$ projected on the vertical plane (white arrows). The b/w dashed curve shows optical depth unity and the dot-dashed and solid black contours $\beta = 1$ and 100, respectively. Schaffenberger, Wedemeyer-Böhm, Steiner & Freytag, 2005, in *Chromospheric and Coronal Magnetic Fields*, ESA Publication SP-596

5.1. Wave propagation in a magnetically structured atmosphere

Time sequence of a two-dimensional simulation of magnetoconvection starting with an initial homogeneous vertical magnetic field of 100 G.

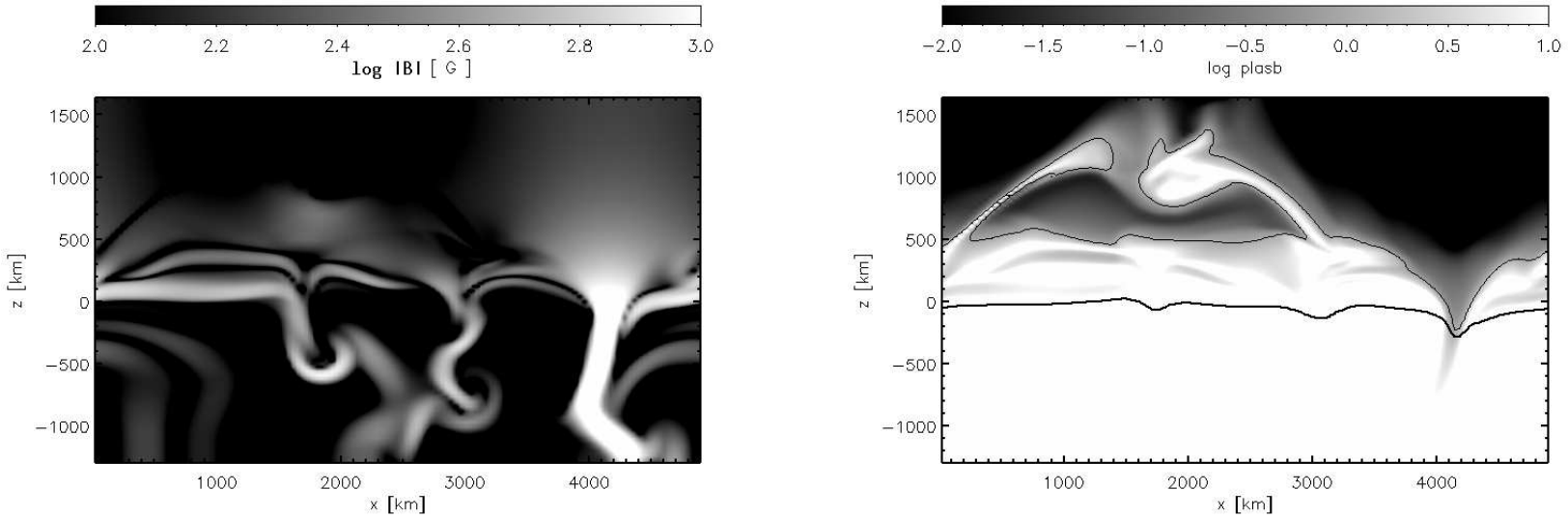

Left: Logarithmic magnetic field strength 1368 s after starting with an initial homogeneous vertical field of 100 G. *Right:* Logarithm of thermal to magnetic energy density (plasma-β) together with the conour of $\beta = 1$.

Wave propagation in a magnetically structured atmosphere (cont.)

Residual velocity amplitude due to an oscillatory velocity perturbation along the bottom

$$v_z(t) = v_0 \sin(2\pi(t - t_0)\nu)$$

with an amplitude of $v_0 = 50$ m/s and a frequency of $\nu_0 = 20$ mHz from $t = 1200$ s to $t = 1450$ s. Note the fast magnetic wave that gets refracted.

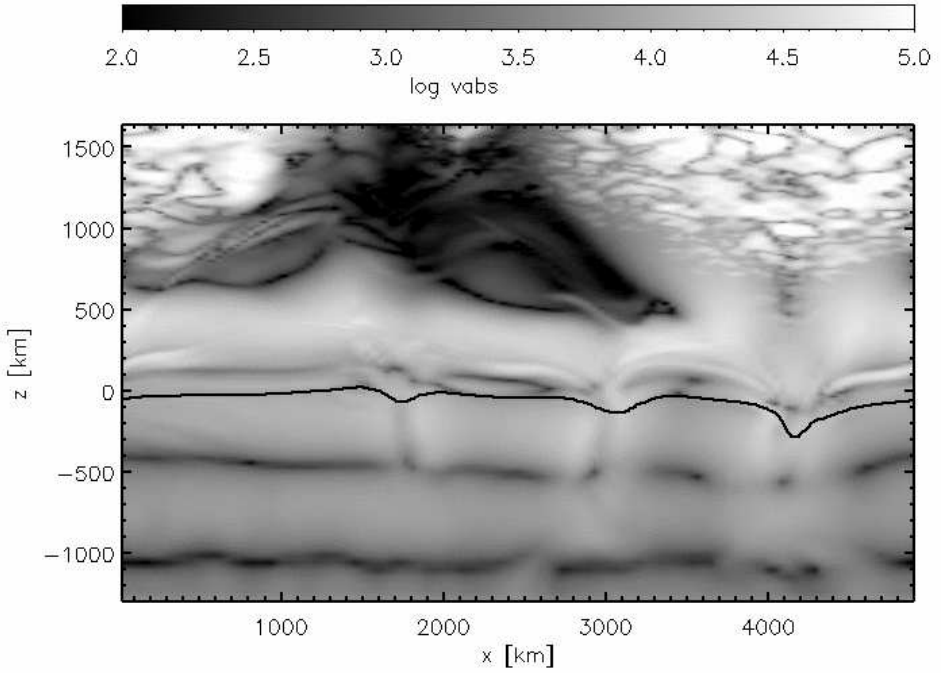

From *Steiner, Vigeesh, Krieger et al.: 2007, Astron. Nachr. / AN 328, 323*

Wave propagation in a magnetically structured atmosphere (cont.)

Wave travel time vs. canopy height.

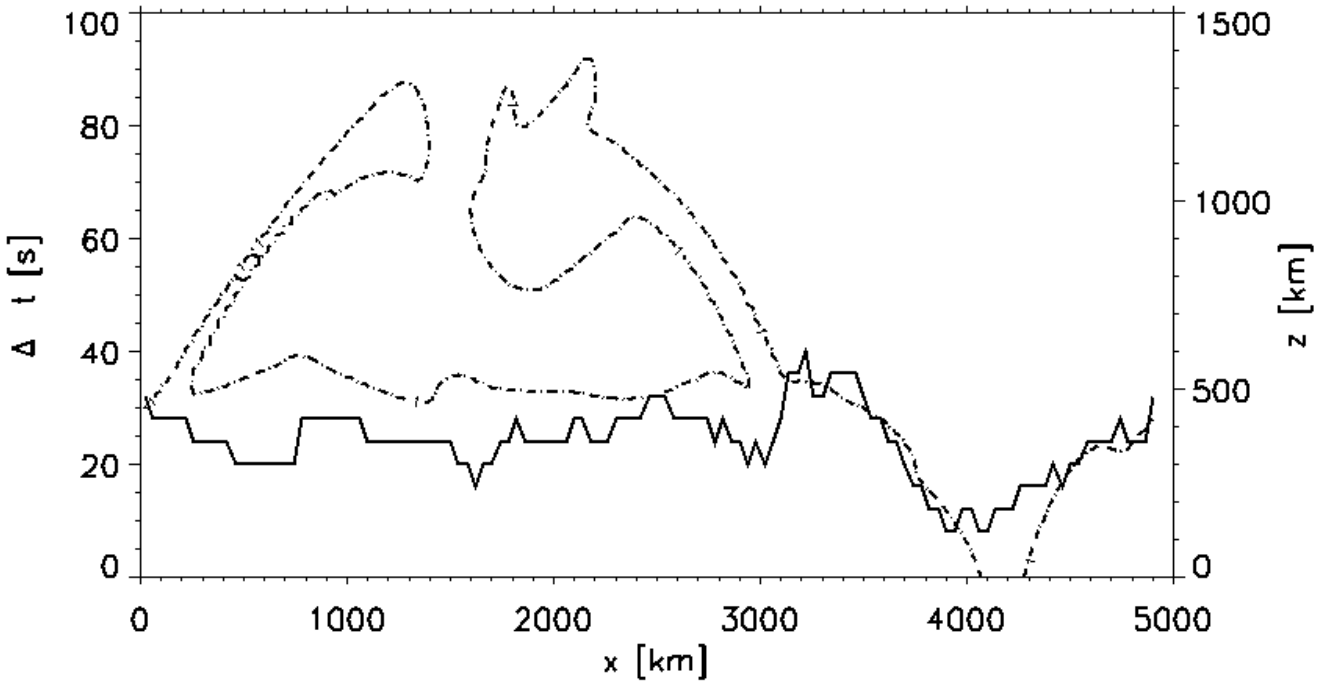

Wave travel time across the layer from $z = 200$ km to $z = 420$ km as a function of horizontal distance (thick solid curve). Superposed is the contour of $\beta = 1$ (magnetic and thermal equipartition), for which the height is indicated in the right hand side ordinate (dash-dotted curve). Note that the travel time markedly decreases where the low β region intrudes this layer.

6. Conclusion

6. Conclusion

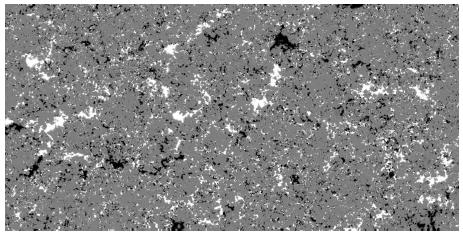

High resolution polarimetry with Hinode

6. Conclusion

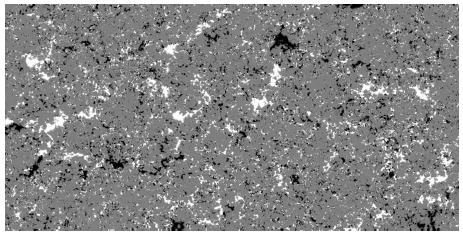

High resolution polarimetry with Hinode

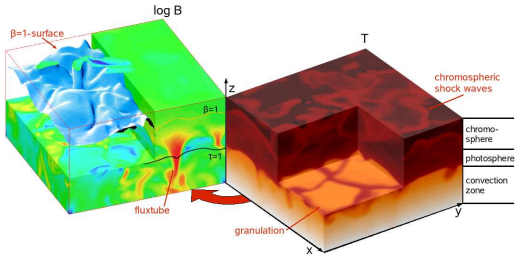

State of the art 3-D MHD-code for the numerical simulation of near surface magnetoconvection

6. Conclusion

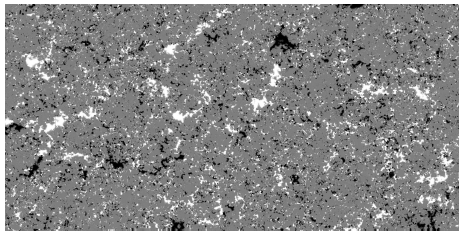

High resolution polarimetry with Hinode

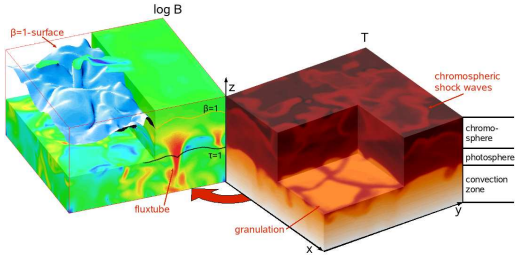

State of the art 3-D MHD-code for the numerical simulation of near surface magnetoconvection

$\frac{\partial B_{x,y,z}}{\partial z} = 0$

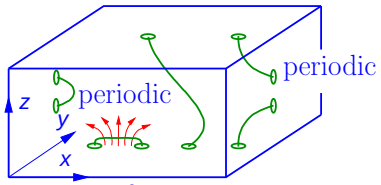

outflow: $\frac{\partial B_{x,y,z}}{\partial z} = 0$

inflow: $B_y = B_z = 0, B_x = \text{const.}$

Two runs with different initial and boundary conditions

Conclusion (cont.)

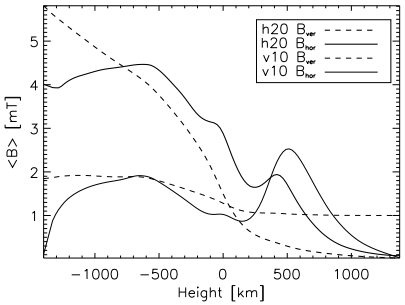

Strong horizontal fields in numerical simulations of the internetwork

Conclusion (cont.)

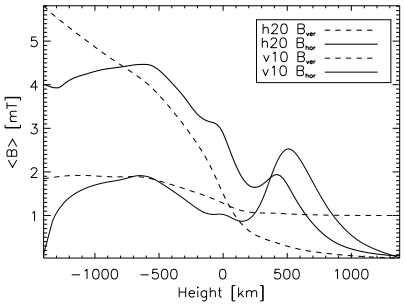

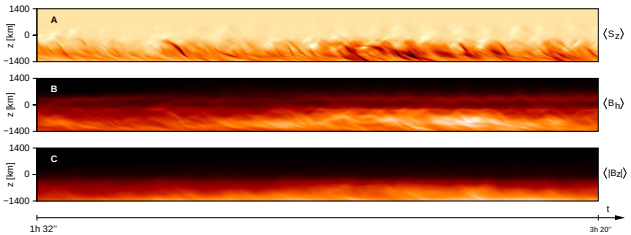

Strong horizontal fields in numerical simulations of the internetwork

$\tau = 1$-surface constitutes a separatrix for the Poynting flux

Conclusion (cont.)

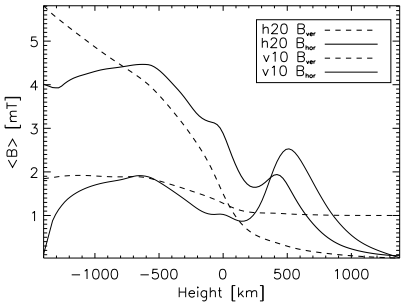

Strong horizontal fields in numerical simulations of the internetwork

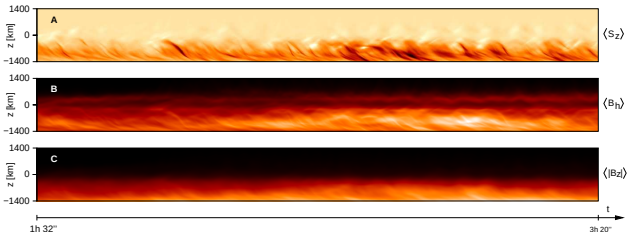

$\tau = 1$-surface constitutes a separatrix for the Poynting flux

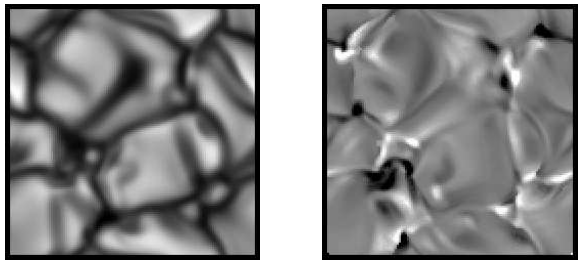

Synthesized Stokes parameters yield $\langle B_{\rm hor}\rangle / \langle B_{\rm ver}\rangle = 1.5 \ldots 2.8$

Conclusion (cont.)

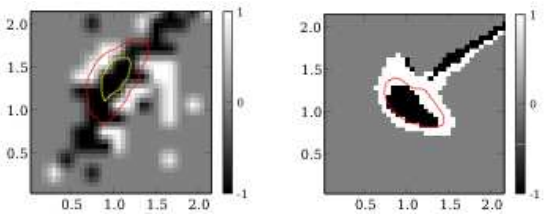

Peculiar pattern of positive area asymmetry of Stokes-V profiles in the periphery of internetwork magnetic elements .....

Conclusion (cont.)

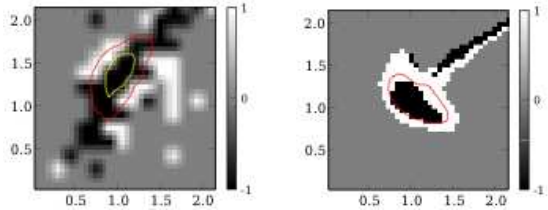

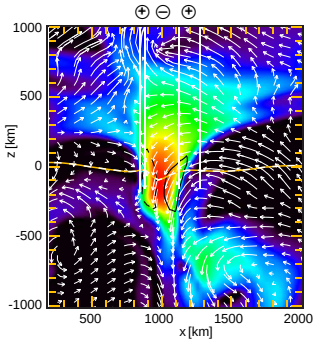

Peculiar pattern of positive area asymmetry of Stokes-V profiles in the periphery of internetwork magnetic elements .....

..... due to their funnel shaped magnetic boundary layer

Conclusion (cont.)

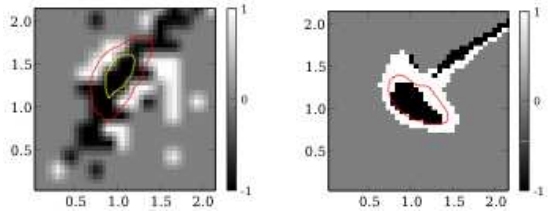

Peculiar pattern of positive area asymmetry of Stokes-V profiles in the periphery of internetwork magnetic elements .....

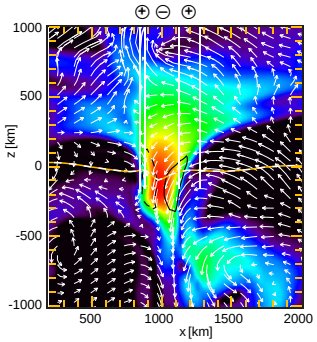

..... due to their funnel shaped magnetic boundary layer

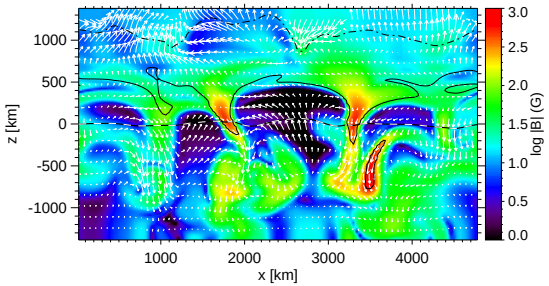

The magnetic field of the internetwork chromosphere

Conclusion (cont.)

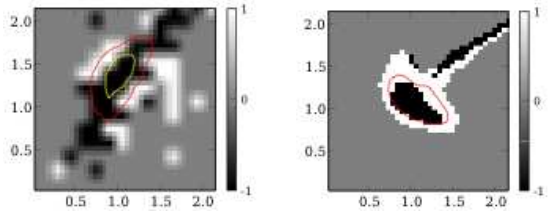

Peculiar pattern of positive area asymmetry of Stokes-V profiles in the periphery of internetwork magnetic elements .....

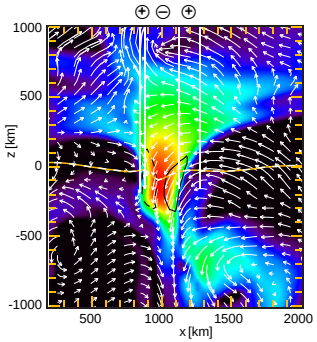

..... due to their funnel shaped magnetic boundary layer

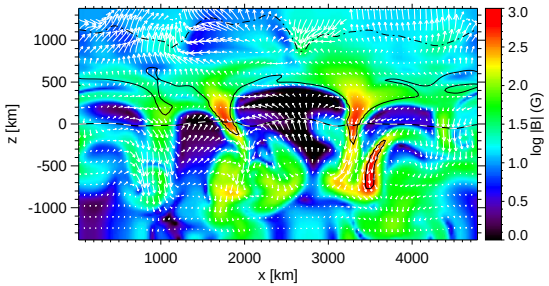

The magnetic field of the internetwork chromosphere

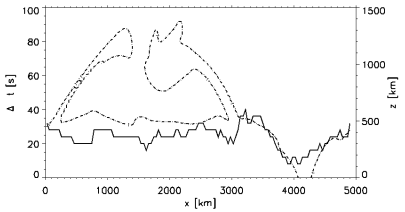

Feasibility of atmospheric magneto-seismology

Table of content